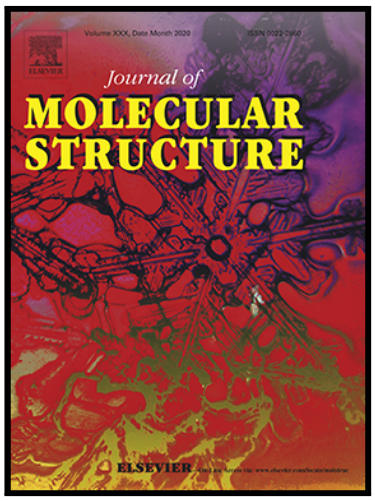

CONFORMATIONAL SEARCH, STRUCTURAL ANALYSIS, VIBRATIONAL PROPERTIES, REACTIVITY STUDY AND AFFINITY TOWARDS DNA OF THE NOVEL INSECTICIDE FLONICAMID

Pablo F. Corregidor , María A Zígolo , Emilce E. Ottavianelli

PII: S0022-2860(21)00761-4
DOI: https://doi.org/10.1016/j.molstruc.2021.130628
Reference: MOLSTR 130628

To appear in: *Journal of Molecular Structure*

Received date: 11 March 2021
Revised date: 15 April 2021
Accepted date: 3 May 2021

Please cite this article as: Pablo F. Corregidor , María A Zígolo , Emilce E. Ottavianelli , CONFORMATIONAL SEARCH, STRUCTURAL ANALYSIS, VIBRATIONAL PROPERTIES, REACTIVITY STUDY AND AFFINITY TOWARDS DNA OF THE NOVEL INSECTICIDE FLONICAMID, *Journal of Molecular Structure* (2021), doi: https://doi.org/10.1016/j.molstruc.2021.130628

CONFORMATIONAL SEARCH, STRUCTURAL ANALYSIS, VIBRATIONAL PROPERTIES, REACTIVITY STUDY AND AFFINITY TOWARDS DNA OF THE NOVEL INSECTICIDE FLONICAMID

Pablo F. Corregidor[1*], María A Zígolo[2] and Emilce E. Ottavianelli[3].

[1]*Facultad de Ingeniería, Instituto de Investigaciones para la Industria Química – INIQUI, Centro Científico Tecnológico (CCT) Salta-Jujuy, Consejo de Investigaciones de la Universidad Nacional de Salta (CIUNSa), Consejo Nacional de Investigaciones Científicas y Técnicas (CONICET), Universidad Nacional de Salta (UNSa), Av. Bolivia 5150, A4408FVYA Salta, Argentina.*

[2]*Facultad de Ciencias Naturales, Instituto de Investigaciones para la Industria Química – INIQUI, Centro Científico Tecnológico (CCT) Salta-Jujuy, Consejo Nacional de Investigaciones Científicas y Técnicas (CONICET), Universidad Nacional de Salta (UNSa), Av. Bolivia 5150, A4408FVYA Salta, Argentina.*

[3]*Facultad de Ciencias Exactas, Instituto de Investigaciones para la Industria Química – INIQUI, Consejo de Investigaciones de la Universidad Nacional de Salta (CIUNSa), Universidad Nacional de Salta (UNSa), Av. Bolivia 5150, A4408FVYA Salta, Argentina*

* Corresponding author. Tel.: +54 387 4255391; fax: +54 387 4251006

E-mail address: pcorregidor@unsa.edu.ar (P.F. Corregidor).

GRAPHICAL ABSTRACT

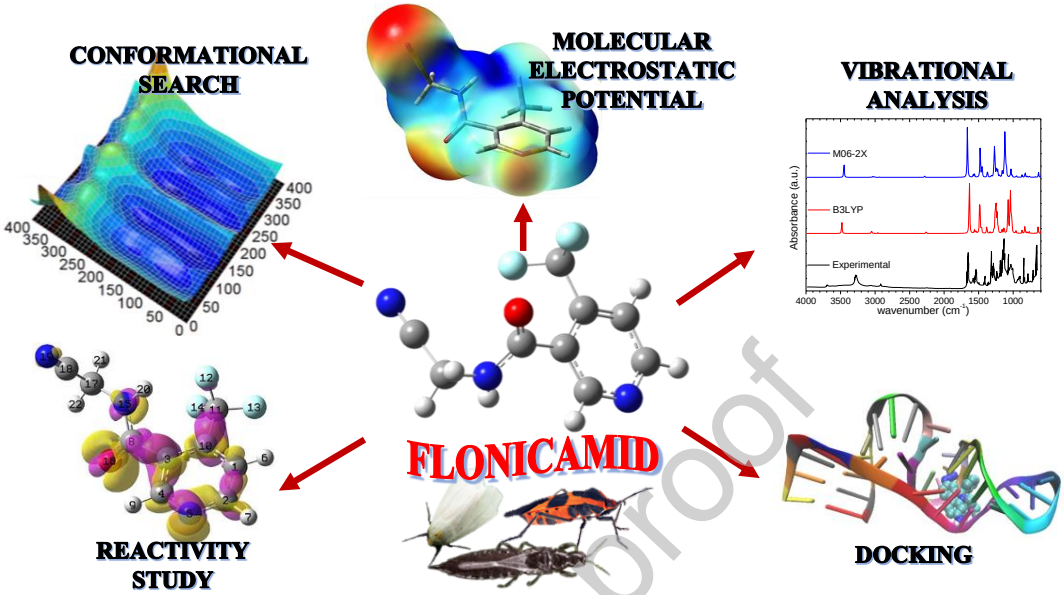

HIGHLIGHTS

- Eight stable conformers were found during a conformational search of flonicamid.
- The calculated absorption spectra exhibits two peaks in the UV region.
- The reactivity study agrees with the traditional reactivity of pyridines.
- High binding energy between flonicamid and a DNA sequence was evidenced by docking.

ABSTRACT

This work deals with the study of structural properties, vibrational analysis, and reactivity of the novel insecticide flonicamid. Eight different minimum energy conformers were found during a conformational search and subsequent geometry optimizations at different levels of theory. The analysis of the PES leads to eight zones of minimum energy due to the

scan of selected dihedral angles, which agrees with the structure of the eight most stable conformers found in the conformational search. The vibrational analysis and a complete assignment of the vibrational modes were performed, evidencing a good correlation with the experimental reported data. Furthermore, to predict the reactivity of flonicamid, different descriptors were analyzed. Finally, results obtained from docking analysis suggested that due to the molecular interaction with a sequence of DNA, the possible carcinogenic effects of flonicamid and three of its most important metabolites must be evaluated experimentally.

KEYWORDS: Flonicamid; Conformational search; Vibrational analysis; Reactivity study; Docking analysis.

1. INTRODUCTION

Flonicamid, which IUPAC name is *N*-cyanomethyl-4-(trifluoromethyl)nicotinamide, is a selective systemic pesticide against hemipterous pests that interferes in the alimentary behavior of some insects, thus quickly inhibiting feeding of a wide range of aphids and other species of sucking insects. [1] Due to its exclusive chemical structure, flonicamid, is considered the unique component of its family and thus represents a novel class of pesticide for controlling both nymph and adult stages of aphids that are resistant to various insecticides. [2] Recently, the group of Bloomquist [3] reported its toxicity in certain mosquitoes and its activity against other insects are also well known, including whiteflies, thrips and planthoppers I5K (n.d.). It´s chemical structure (Fig. 1) consists of a pyridine ring substituted by a trifluoromethyl group in position 4, thus becoming the only member of the trifluoromethylnicotinamide class of insecticides. [4]

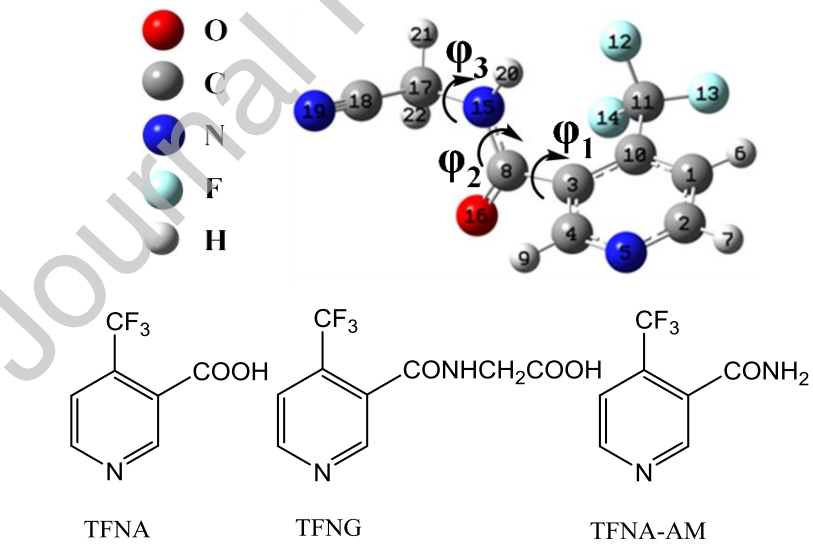

Figure 1. Molecular structure and numbering for flonicamid (up) and its metabolites (down).$\boldsymbol{\varphi}_1$, $\boldsymbol{\varphi}_2$ and $\boldsymbol{\varphi}_3$ are C10–C3–C8–O16, C3–C8–N15–C17, H20–N15–C17–H21 dihedral angles, respectively.

Moreover, the pyridine-3-carboxamide (nicotinamide) group exists in many important compounds, i.e., in cells as nicotinamide adenine dinucleotide (NAD) and nicotinamide adenine dinucleotide phosphate (NADP) which are coenzymes in a wide variety of enzymatic oxidation–reduction reactions. Therefore, this basic structure has been the subject of many experimental and theoretical studies. [5-9]

Besides, it is well known that introducing fluorine into a molecule, it will: i) improve the lipophilicity (in reference to hydrogen parent compound), ii) increase its stability as the C−F bond is much stronger than C−H, iii) modify some physical properties and chemical reactivity due to changes in electronic properties and iv) produce a bioisosteric replacement as the substitution of hydrogen by fluorine closely resemble hydrogen's steric requirement for binding to an active site. [10] Moreover, investigation into the biological activity of a number of 5-substituted pyridalyl derivatives revealed that the trifluoromethyl group is essential for providing the best insecticide action. [11] Previous reports of compounds with insecticidal, mosquito repellent or fungicidal activity, delivered the idea that the amide group within the molecule may improve its stability and provide the ability to establish intermolecular hydrogen bonds with some biological targets. [12]

On the other hand, it is known that continual application of pesticides generate environmental problems as most of them are environmental toxic and hazardous. Pesticides can cause the pollution of soil and water and represent a danger to human health and the balance of ecosystems. [13] Flonicamid is used to regulate the pest in corps of cabbage, cotton, wheat and potatoes. [14] It can create significant environmental issues attributed to its toxic and carcinogenic nature. Moreover, this pesticide has a high stability and solubility (5.2 g/L at 20 °C) in water. Due to this, it can create significant environmental issues. On

the other hand, flonicamid metabolizes and yield different degradation products, some of the most important are N–(4–trifluoromethylnicotinoyl) glycine (TFNG), 4–trifluoromethylnicotinic acid (TFNA) and 4–trifluoromethylnicotinamide (TFNA-AM), as shown in Fig. 1. [15] Different countries such as the USA, Japan, China, and others have established strict limits for flonicamid and its metabolites in cultivation for human consumption. [1, 16, 17] This is a very important topic since these differences in normative between countries can cause barriers to the international trade in agricultural commodities. [18] As a result, many methods were developed for the detection of flonicamid and its metabolites in crops. Nonetheless, the information on the dissipation behaviors and terminal residues of flonicamid and its metabolites (TFNA, TFNA-AM and TFNG) in corps and soil is still scarce so far as well as its effects in human health. [19]

In that sense, Sahu et al. [14] recently reported the chemical determination of flonicamid in various environmental and vegetable samples using UV–Visible and FTIR techniques based on the hydrolysis of flonicamid and bromination followed by a reaction with KI and leucocrystal violet. They concluded that the method must be validated to explore the effect of interfering compounds on the pesticide detection and might offer a good option to be introduced into real on-site applications. Consequently, counting with spectral information about some of the most used analytical techniques may result mandatory to contribute with the detection, identification, and quantification of flonicamid. To the best of our knowledge, there are no reports of its UV-vis spectra or X-ray diffraction data, and we could not find a complete assignment of the bands observed in the infrared spectra to completely identify this substance in all the media in which it can be found.

In this context, the aim of this work is to contribute with theoretically predicted structural parameters that may give suitable information about the geometry and properties of flonicamid. Thus, to have a proper insight of the structural profile of the compound, a detailed conformational search using 3D potential energy scan was done by varying selected dihedral angles and confirming its relative conformational stability. Afterwards, we performed a complete assignment of the bands observed in the infrared spectra and calculated the electronic absorption spectrum. Additionally, we implemented a careful reactivity study based on Molecular Electrostatic Potential, Fukui functions, dual descriptor, and their corresponding condensed descriptors to predict the reactivity and the behavior of the studied molecule in any media. Finally, we evaluated the binding affinities of flonicamid and three of its main detected metabolites (TFNG, TFNA, TFNA-AM) in culture to DNA, using docking analysis, which may exhibit a direct implication on its possible carcinogenic effect.

2. COMPUTATIONAL METHODS

The conformational space of flonicamid was studied theoretically by systematic variation of all the dihedral angles using the molecular dynamic simulations module with the aid of the MM^{+} force field, both available in the HyperChem package. [20] Different geometries in this conformational space have been generated by heating from 0 to 900 K in 0.1 ps. During the simulation, the temperature of annealing was kept constant by coupling the system to a simulated thermal bath with a bath relaxation time of 0.5 ps. The time step for the simulation was 0.5 fs. After an equilibration period of 10 ps, a 500 ps-long simulation was started saving the Cartesian coordinates at every 10 ps. These geometries were then optimized to an energy gradient of less than 0.005 kJ $mol^{-1}Å^{-1}$ using the semiempirical

method AM1, due to its demonstrated level of prediction in the theoretical study of geometrical and electronic characteristics of heteroaromatic compounds. [21] The as-obtained twenty geometries were then taken as initial guess for geometry optimization and electronic structure calculation using a molecular-orbital approach within the framework of spin-polarized density functional theory [22] with a double zeta 6-31G basis set, employing the KS exchange along with the Vosko-Wilk-Nussair [23] parameterization of homogeneous electron gas data, due to Ceperley and Alder [24] for the correlation potential. We shall henceforth refer to this specific local spin density approach (LSDA) as SVWN.

We have also carried out calculations that go beyond the LSDA and considering gradient corrections. In this case, we have implemented density functional theory (DFT) using B3LYP [25, 26] and M06–2X [27] functionals with polarized triple-zeta 6-311+G(d,p) [28, 29] basis set. The exceedingly popular B3LYP exchange-correlation functional mixes a certain amount of the exact Hartree-Fock exchange energy into the exchange and correlation obtained from Beckes's exchange functional, while the M06–2X functional was previously found to have a favorable trade-off between experimental accuracy and computational efficiency in organic compounds. [27] Moreover, the inclusion of solvation effects was incorporated by means of the polarized continuum model (PCM) in both DFT types of calculations.

The nature of the critical points on the potential surface was determined by inspection of the corresponding calculated Hessian matrix. All ground-state structures were equilibrium states without imaginary frequencies.

Thus, with the lowest energy conformer obtained at B3LYP/6-311+G(d,p) level, a potential energy surface (PES) scan for the rotation around the C3–C8 and C17–N15 bonds was done at the same level of theory, taking steps of 30° to obtain 169 geometries

Time Dependent Density Functional Theory (TD-DFT) has been applied to simulate the electronic absorption spectra of flonicamid at the B3LYP/6-311+G(d,p) level considering the PCM method (solvent=water) starting from the optimized geometry of the most stable conformer found at the same level of theory. Surfaces were generated with an isovalue of 0.02 and visualized using the open-source molecular builder and visualization tool Avogadro v1.2.0. [30]

The calculated harmonic vibrational frequencies have been scaled by 0.9613 [31] and 0.944 [32] for 6-311+G(d,p) basis set using B3LYP and M06-2X levels, respectively. The calculated vibrational frequencies were assigned via potential energy distribution (PED) analysis of all the fundamental vibration modes by the use of the VEDA 4 program [33, 34], which has been implemented in previous studies by many researchers. [35-38] All the vibrational assignments were based on the most stable conformer obtained at B3LYP/6-311+G(d,p) level of calculations. Vibrational modes were expressed in terms of internal coordinates, i.e., bond-stretching (ν), angular bending (β), out-of-plane bending (ω) and torsion (τ) coordinates.

With the optimized geometry at B3LYP/6-311+G(d,p) level of theory, we have calculated chemical reactivity parameters based upon Conceptual Density Functional Theory (CDFT). This methodology has been employed widely to compare the chemical reactivity of different types of chemical systems. Although these parameters are not physically

observable, they are highly successful to predict chemical reactions with rigorous mathematical models. Global and atomic indices of reactivity were calculated at B3LYP/6-31G(d) level of theory using the Multiwfn package. [39] Condensed Fukui function and dual descriptor were calculated based on electron density and Hirshfeld charge as it has been demonstrated to be the best choice for evaluating the condensed Fukui function. [40]

All the DFT and TD-DFT studies were conducted using the Gaussian 16 [41] software package implemented in the SEAGrid portal. [42-44]

The coordinates and structure factors for the crystalline structure of the synthetic DNA dodecamer d(CpGpCpGpApApTpTpCpGpCpG) used in this study, was taken from the Protein Data Bank (PDB ID: 1BNA). [45]

The three-dimensional structure of the three main metabolites of flonicamid and the control compound ethidium bromide were obtained from the PubChem database (https://pubchem.ncbi.nlm.nih.gov/): TFNG (Glycine, N-[[4-(trifluoromethyl)-3-pyridinyl] carbonyl]) (CID: 46835486); TFNA (4-(Trifluoromethyl) nicotinic acid) (CID: 2777549); TFNA-AM (4-(Trifluoromethyl) nicotinamide) (CID: 2782643) and ethidium bromide (CID: 14710). The most stable conformer of flonicamid found at M06–2X/6-311+G(d,p) level of theory (water PCM solvated) has been used for the docking analysis.

Docking calculations were carried out with Autodock 4.2 program, which uses Lamarckian genetic algorithm (LGA) for calculations. [46] Number of runs was set to 200 for each analyzed case. The Autodock 4.2 program was applied considering all rotatable bonds for ligands and DNA sequence as a rigid structure. For the location and extent of the 3D area, the search space was defined by specifying a center, the number of points at each dimension and the points between spaces.

The grid box center coordinates corresponded to the O atom of the H_2O molecule 410: x (11.346), y (24.175), and z (4.920). Dimensions of the grid box were 60 x 80 x 126 and a point spacing of 0.375 Å.

Prior to the docking analysis, water molecules were removed from the DNA sequence. Polar hydrogen atoms were added and Gasteiger atom charges were assigned to DNA atoms. Other parameters were set to default values.

The 200 conformers found for each compound using the Autodock program were grouped into clusters and ordered according to a ranking, which was determined by the stability of the DNA-ligand complexes within each cluster. Clustering of the 200 conformers was done according to their similar conformation adopted inside the DNA sequence. The criterion used to evaluate such similarity was the Residue Mean Quadratic Square Root Deviation (RMSD). These residues were obtained through the difference between the atom coordinates of a given conformer with respect to the cluster to which the most stable conformer belongs. Each cluster grouped conformers with RMSD lower or equal to 2.0 Å.

For visualization of protein-ligand complexes the software Visual Molecular Dynamics 1.9.1 (VMD) was used (Theoretical and Computational Biophysics Group, University of Illinois).

Statistical software R (https://cran.r-project.org/) with the Rstudio IDE (https://rstudio.com/) was implemented for processing data.

3. RESULTS AND DISCUSSION

3.1.Structural analysis

The molecular structure of flonicamid as well as the numbering used in this article are summarized in Fig. 1. After the geometry optimization of the twenty conformers obtained at SVWN level, only eight different conformers were found, each of them differing in ± 0.06 eV (~1.5 kcal/mol). These conformers were taken as inputs for geometry optimization at DFT level.

The chemical structures of the eight conformers obtained at M06-2X/6-311+G(d,p) in solvent are shown in Fig. S1 (Electronic Supplementary Information), while some selected geometrical parameters calculated by both M06-2X and B3LYP functional with the 6–311+G(d,p) basis set (in gas phase and solvent) are resumed in Table 1. IUPAC's rules were applied to establish a denomination for the eight as-found conformers in Table 1, as explained in section S1. For each method, the conformer having the lowest energy was taken as reference to compute the relative energy of the different conformational arrangements. The range of relative energy was calculated as follow: $E_{rel,i} = E_i - E_{reference}$. In the later: $E_{rel,i}$ is the relative energy of conformer "i", E_i: energy of conformer "i" and $E_{reference}$ is the energy of the most stable conformer obtained at a given theoretical method.

The N-cyanomethylcarboxamide group, bonded to the aromatic ring, contains the most important functional groups in the molecule, and henceforth referred to as the principal chain (–R). According to our calculations, the lowest-energy conformers of flonicamid belong to the C_1 symmetry point group.

The conformations of the eight most stable calculated structures are properly and qualitatively described by the orientation of atoms/groups according to three dihedral

angles: φ_1 (C10–C3–C8–O16), φ_3 (H20–N15–C17–H21) and φ_4 (C1–C10–C11–F). A fourth dihedral angle φ_2 (C3–C8–N15–C1) exhibits the antiperiplanar (*ap*) conformation in all the calculated structure, as will be explained soon in this section. Therefore, it is not considered in the denomination assignment based in the conformation possibilities. Thus, a qualitative description based on these three dihedral angles has been used to assign a denomination for all the as-obtained conformers (Table 1). A detailed analysis of the structural properties (bond lengths and angles) was presented in section S1.

Table 1. Computed properties: bond lengths (**d**), bond angles (**θ**), dihedral angles (**φ**), given in Å and °, as well as denomination and energies (relative to the most stable) for the conformers obtained at different levels of theory in gas phase and solvent.

	Conformer 1				**Conformer 2**				**Conformer 3**				**Conformer 4**			
	B3LYP		M06-2X		B3LYP		M06-2X		B3LYP		M06-2X		B3LYP		M06-2X	
	gas	solvent	gas	solvent	gas	solvent	gas	solvent	gas	solvent	gas	Solvent	gas	solvent	gas	solvent
$\mathbf{d_{C2\text{-}N5}}$	1.3326	1.3342	1.3285	1.3300	1.3344	1.3362	1.3304	1.3322	1.3345	1.3364	1.3308	1.3324	1.3344	1.3362	1.3304	1.3322
$\mathbf{d_{C11\text{-}F12}}$	1.3438	1.3519	1.3308	1.3380	1.3660	1.3588	1.3508	1.3453	1.3663	1.3592	1.3520	1.3458	1.3467	1.3510	1.3348	1.3391
$\mathbf{d_{C8\text{-}O16}}$	1.2154	1.2242	1.2076	1.2173	1.2182	1.2248	1.2100	1.2178	1.2182	1.2247	1.2097	1.2178	1.2181	1.2248	1.2100	1.2178
$\mathbf{d_{C8\text{-}N15}}$	1.3714	1.3588	1.3703	1.3547	1.3664	1.3569	1.3637	1.3531	1.3676	1.3570	1.3655	1.3526	1.3664	1.3569	1.3637	1.3531
$\mathbf{d_{N15\text{-}H20}}$	1.0089	1.0097	1.0092	1.0099	1.0085	1.0094	1.0085	1.0096	1.0088	1.0096	1.0089	1.0095	1.0085	1.0094	1.0085	1.0096
$\mathbf{d_{N15\text{-}C17}}$	1.4549	1.4518	1.4478	1.4460	1.4531	1.4519	1.4456	1.4455	1.4537	1.4523	1.4462	1.4462	1.4531	1.4519	1.4456	1.4455
$\mathbf{d_{C17\text{-}H21}}$	1.0947	1.0906	1.0916	1.0883	1.0946	1.0906	1.0910	1.0886	1.0920	1.0914	1.0907	1.0910	1.0921	1.0912	1.0906	1.0911
$\mathbf{d_{C17\text{-}C18}}$	1.4665	1.4728	1.4711	1.4756	1.4678	1.4726	1.4732	1.4754	1.4684	1.4724	1.4729	1.4749	1.4678	1.4736	1.4732	1.4754
$\mathbf{d_{C18\text{-}N19}}$	1.1524	1.1526	1.1477	1.1481	1.1524	1.1526	1.1477	1.1480	1.1523	1.1525	1.1477	1.1480	1.1524	1.1526	1.1477	1.1480
$\mathbf{\theta_{C3\text{-}C8\text{-}O16}}$	122.26	121.99	122.30	122.18	120.36	120.85	120.83	121.34	120.20	120.81	120.79	121.34	120.36	120.85	120.83	121.34
$\mathbf{\theta_{C8\text{-}N15\text{-}H20}}$	119.32	119.84	118.81	120.30	120.15	120.03	120.14	120.61	120.11	120.24	119.83	121.00	120.15	120.03	120.14	120.61
$\mathbf{\theta_{N15\text{-}C17\text{-}H21}}$	111.15	109.31	110.92	109.41	110.93	109.26	110.27	109.33	107.14	109.57	107.74	110.32	107.24	109.45	107.93	109.96
$\mathbf{\theta_{C17\text{-}C18\text{-}N19}}$	178.35	179.59	176.29	179.67	178.71	179.63	178.72	179.77	178.53	179.67	178.71	179.85	178.71	179.63	178.72	179.77
$\mathbf{\theta_{F13\text{-}C11\text{-}F12}}$	106.90	106.52	107.09	106.76	106.40	106.63	106.59	106.86	106.43	106.68	106.68	106.92	107.36	107.06	107.60	107.38
$\mathbf{\varphi_1}$	302.68	303.79	310.19	308.87	127.76	119.81	130.88	124.25	129.29	117.41	128.64	120.76	232.24	240.19	229.12	235.75
$\mathbf{\varphi_2}$	179.75	176.41	182.09	179.72	179.53	179.57	181.53	179.90	179.65	181.99	173.85	178.33	180.48	180.43	178.47	180.10
$\mathbf{\varphi_3}$	73.07	33.75	65.84	23.38	73.07	59.79	47.91	20.72	179.36	215.94	186.19	226.09	182.42	211.00	193.40	220.07
$\mathbf{\varphi_4}$	262.56	261.94	259.78	260.48	254.70	256.66	256.62	257.64	254.67	256.40	258.01	258.26	225.02	223.20	223.38	222.26
Denomin. (ϕ_1 ϕ_3 ϕ_4)	-sc +sc -ac	-sc +sc -ac	-sc +sc -ac	-sc sp -ac	+ac +sc -ac	+ac +sc -ac	+ac +sc -ac	+ac sp -ac	+ac ap -ac	+ac -ac -ac	+ac ap -ac	+ac -ac -ac	-ac ap -ac	-ac -ac -ac	-ac ap -ac	-ac -ac -ac
Relative E. (eV)	0.051	0.000	0.059	0.000	0.000	0.020	0.000	0.020	0.022	0.025	0.008	0.016	0.000	0.020	0.000	0.020

(Table 1. Continuation…)

	Conformer 5				**Conformer 6**				**Conformer 7**				**Conformer 8**			
	B3LYP		M06-2X		B3LYP		M06-2X		B3LYP		M06-2X		B3LYP		M06-2X	
	gas	solvent	gas	solvent	gas	solvent	gas	solvent	gas	solvent	gas	Solvent	gas	solvent	gas	solvent
$\mathbf{d_{C2\text{-}N5}}$	1.3345	1.3364	1.3308	1.3324	1.3327	1.3343	1.3284	1.3300	1.3327	1.3342	1.3285	1.3300	1.3327	1.3343	1.3284	1.3932
$\mathbf{d_{C11\text{-}F12}}$	1.3435	1.3451	1.3326	1.3337	1.3528	1.3507	1.3417	1.3397	1.3438	1.3518	1.3308	1.3380	1.3438	1.3524	1.3302	1.3382
$\mathbf{d_{C3\text{-}C8}}$	1.5119	1.5103	1.5073	1,2178	1.5091	1.5081	1.5040	1.5025	1.5087	1.5080	1.5039	1.5019	1.5087	1.5081	1.5040	1.5025
$\mathbf{d_{C8\text{-}N15}}$	1.3676	1.3569	1.3655	1.3523	1.3702	1.3579	1.3671	1.3532	1.3714	1.3588	1.3703	1.3547	1.3714	1.3579	1.3671	1.3532
$\mathbf{d_{N15\text{-}H20}}$	1.0088	1.0096	1.0089	1.0095	1.0088	1.0095	1.0087	1.0094	1.0089	1.0097	1.0092	1.0092	1.0089	1.0095	1.0087	1.0094
$\mathbf{d_{N15\text{-}C17}}$	1.4537	1.4527	1.4462	1.4462	1.4538	1.4522	1.4472	1.4463	1.4549	1.4518	1.4478	1.4460	1.4549	1.4522	1.4472	1.4463
$\mathbf{d_{C17\text{-}H21}}$	1.0941	1.0902	1.0909	1.0882	1.0924	1.0914	1.0913	1.0914	1.0926	1.0911	1.0911	1.0907	1.0926	1.0904	1.0928	1.0884
$\mathbf{d_{C17\text{-}C18}}$	1.4684	1.4724	1.4729	1.4749	1.4669	1.4724	1.4693	1.4745	1.4665	1.4727	1.4711	1.4756	1.4665	1.4724	1.4693	1.4745
$\mathbf{d_{C18\text{-}N19}}$	1.1523	1.1525	1.1477	1.1480	1.1524	1.1526	1.1477	1.1480	1.1524	1.1526	1.1477	1.1481	1.1524	1.1526	1.1477	1.1480
$\mathbf{\theta_{C3\text{-}C8\text{-}O16}}$	120.20	120.81	120.79	121.34	122.20	121.89	122.28	122.22	122.26	122.00	122.30	122.18	122.26	121.89	122.28	122.21
$\mathbf{\theta_{C8\text{-}N15\text{-}H20}}$	120.11	120.24	119.83	120.92	119.45	120.06	119.55	120.86	119.31	119.84	118.81	120.30	119.31	120.06	119.55	120.86
$\mathbf{\theta_{N15\text{-}C17\text{-}H21}}$	110.70	109.17	110.56	109.34	107.03	109.48	107.33	110.37	107.04	109.34	107.41	109.99	111.29	109.33	111.66	109.29
$\mathbf{\theta_{C17\text{-}C18\text{-}N19}}$	178.53	179.67	178.71	179.85	178.71	179.75	178.62	179.91	178.35	179.59	178.28	176.67	178.35	179.75	178.62	179.91
$\mathbf{\theta_{F13\text{-}C11\text{-}F12}}$	106.43	106.68	106.68	106.92	106.73	106.73	106.94	106.91	108.02	107.33	108.41	107.66	107.86	107.26	108.29	107.65
$\mathbf{\phi_1}$	230.71	242.59	231.36	239.24	300.72	301.64	309.27	308.33	57.32	56.24	49.78	51.13	59.28	58.36	50.73	51.67
$\mathbf{\phi_2}$	180.35	178.01	186.15	181.67	178.60	178.19	178.47	178.44	180.24	183.63	177.92	180.27	181.40	181.82	181.53	181.56
$\mathbf{\phi_3}$	63.07	25.74	55.24	14.43	181.07	215.35	179.59	230.19	169.28	208.14	175.61	217.33	61.46	26.29	62.08	10.31
$\mathbf{\phi_4}$	225.10	223.23	221.70	221.36	262.06	262.80	260.06	261.07	97.45	98.09	100.21	99.52	97.45	97.20	99.94	98.93
Denomin. (ϕ_1 ϕ_3 ϕ_4)	-ac +sc -ac	-ac sp -ac	-ac +sc -ac	-ac sp -ac	-sc ap -ac	-sc -ac -ac	-sc ap -ac	-sc -ac -ac	+sc ap +ac	+sc ap +ac	+sc ap +ac	+sc -ac +ac	+sc +sc +ac	+sc sp +ac	+sc +ac	+sc sp +ac
Relative E. (eV)	0.022	0.025	0.008	0.016	0.037	0.002	0.046	0.011	0.051	0.000	0.059	0.000	0.037	0.002	0.046	0.011

Before proceeding with the reading of this article, the reader is referred to section S1 (Supplementary Information) for a better understanding of the geometrical properties' analysis.

Table S1 exhibits the averaged structural properties for the studied molecule, which are in good agreement with experimental values for selected references compounds having a similar structure (Fig. S3).

To establish the most stable conformations that may exhibit the studied molecule, we will concentrate our analysis only in the four dihedral angles that could rotate groups leading to different conformers. As was mentioned, these dihedrals are C10–C3–C8–O16, C3–C8–N15–C17, H20–N15–C17–H21 and C1–C10–C11–F named as φ_1, φ_2, φ_3 and φ_4, respectively.

- *φ_1: C10–C3–C8–O16 dihedral angle*: this dihedral brings information about the C=O with respect to the trifluoromethyl group and it is also related to the planarity between the carbonyl group and the aromatic ring. In a synperiplanar (*sp*) conformation of φ_1, the carbonyl group is conjugated with the aromatic ring when the C=O points in the same direction as the trifluoromethyl group. On the other hand, if φ_1 is antiperiplanar (*ap*), then the carbonyl is also conjugated with the aromatic ring but pointing to an opposite direction about the $-CF_3$ group. Intermediate situations in which φ_1 is synclinal (±*sc*) or anticlinal (±*ac*) broke the conjugation between the pyridine ring and the C=O group. If $0° < \varphi_1 < 90°$ or $270° < \varphi_1 < 360°$, then both groups (C=O and $-CF_3$) pointed in the same direction (i.e., up, as represented in Fig. 2A). On the other hand, when $90° < \varphi_1 < 270°$, they pointed in opposite directions (one is up and the other is down). From

the results obtained in this paper, it is clear that the C10–C3–C8–O16 is not planar, which agrees with previous reports. [47]

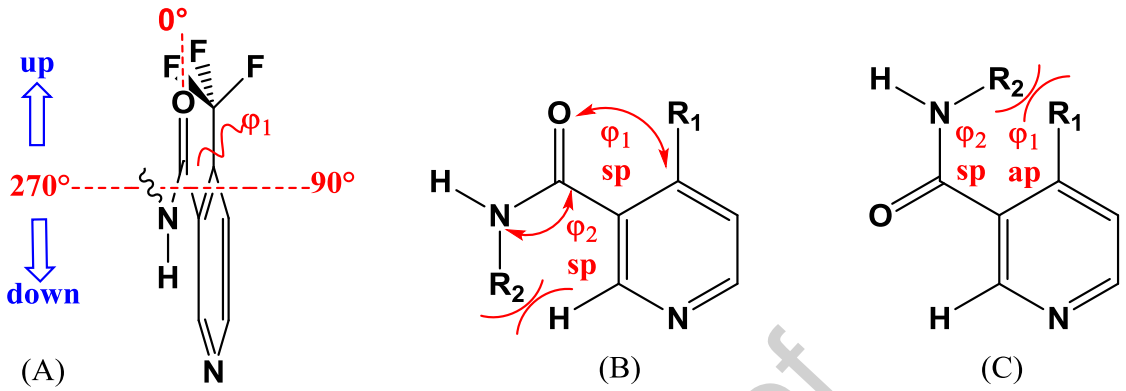

Figure 2. (A) Side view of the studied molecule showing aligned configuration (up) of C=O and $–CF_3$. Synperiplanar stereochemistry for φ_2 considering different arrangement for φ_1: (B) synperiplanar and (C) antiperiplanar. R_1= $–CF_3$ group and R_2= $–CH_2CN$.

- *φ_2: C3–C8–N15–C17 dihedral angle*: as was mentioned before, all the 32 most stable geometries (8 for each different method) evidenced the antiperiplanar (*ap*) stereochemistry. In this geometry, the C3 and C17 are in the same plane but pointing out to opposite directions. If we contrarily assume that φ_2 is synperiplanar, then repulsion between groups must be considered, depending on the value for φ_1 (Fig. 2B an d C). For the situation in which φ_1 is also synperiplanar (Fig. 2B), a repulsion between the R_2 group (R_2= $–CH_2CN$) and H9 should be observed. Otherwise, non-favorable interactions concerning R_2 and R_1 (R_1= $–CF_3$) groups may be present for the antiperiplanar disposition of φ_1. Therefore, the synperiplanar stereochemistry for φ_2 is not the most stable situation for φ_1 in antiperiplanar or synperiplanar conformation. A similar conclusion can be arrived by considering the antiperiplanar stereochemistry for φ_2, except that repulsion between H atoms must be considered (similar as the one

observed between H and R_2 in Fig. 2B) for φ_1 synperiplanar and repulsion between H and R_1 (in analogy to the R_1 and R_2 interaction in Fig 2C) for the antiperiplanar conformation of φ_1. Thus, synclinal and anticlinal for φ_1 are the only possible conformations observed in the eight most stable conformers, despite a loss in the planarity.

- *φ_3: H20–N15–C17–H21 dihedral angle*: this dihedral gives information about the stereochemistry of the carbonyl and cyano group between each other. It exhibits all the possible conformations as can be seen from Table 1.

- *φ_4: C1–C10–C11–F dihedral angle*: this dihedral provides evidence about the possible conformations of Fluorine atoms with respect to C1 atom of the aromatic ring. The three F atoms are equivalent for the conformational analysis, due to the rotation around C10–C11 bond. Therefore, only *ac* conformations were evidenced in the eight most stable rotamers for any of the studied methods (Fig. S4).

At this point it should be convenient to notice that the most stable conformations depend on the inclusion of solvent but does not depend on the functional that was implemented in calculations. The most stable geometries obtained in gas phase are conformers 2 and 4 while conformers 1 and 7 turn out to be the most stable in solvent (water).

3.2.Potential Energy Surface (PES) scan

In addition to the trifluoromethyl group, which has been introduced in the molecule to potentiate its insecticide activity, flonicamid has an aromatic ring with a flexible side chain in which at least three different internal rotations can be identified by simple inspection through the molecular skeleton (Fig. 1): rotations around bonds C3–C8, C8–N15 and N15–

C17. As the O=C–N group has an amide nature, the C–N exhibits a partial double bond character. Therefore, this bond is relatively stable and thus possesses a limited flexibility in comparison with other bonds in the side chain. [48] Moreover, this restricted flexibility makes the O=C–N–H group planar.

On the other hand, it has been demonstrated that the antiperiplanar conformation in φ_2 is the only observed in the eight most stable conformers (at all levels of theory studied in this paper). Therefore, internal rotation around the C8–N15 bond is not going to be considered for the conformational analysis. So far, only rotations around N15–C17 and C3–C8 have been scanned to study the associated Potential Energy Surface (PES).

Rotations around the mentioned bonds correspond to variations in C10–C3–C8–O16 and H20–N15–C17–H21 dihedrals angles, which are represented by φ_1 and φ_3, respectively. The as obtained PES is shown in Fig. 3, as well as the associated PES projection. The potential energy surface represents an important and useful tool supporting the visualization and interpretation of the relationship between potential energy and molecular geometry, as well as the understanding of how prediction methods may locate and characterize possible structures of interest.

During the calculation, all the geometrical parameters were relaxed while the φ_1 and φ_3 angles were varied in steps of 30°, obtaining a 13x13 grid. The 3D-plot shows three maxima (M_1, M_2 and M_3) and eight zones of minimum energy (A_1, A_2, A_3 … A_8). The global maximum (M_1) is observed at φ_1=2° and φ_3 =313° (Fig. 4) with an excess of 0.56 eV (12.91 kcal/mol) with respect to the most stable conformer (A_6).

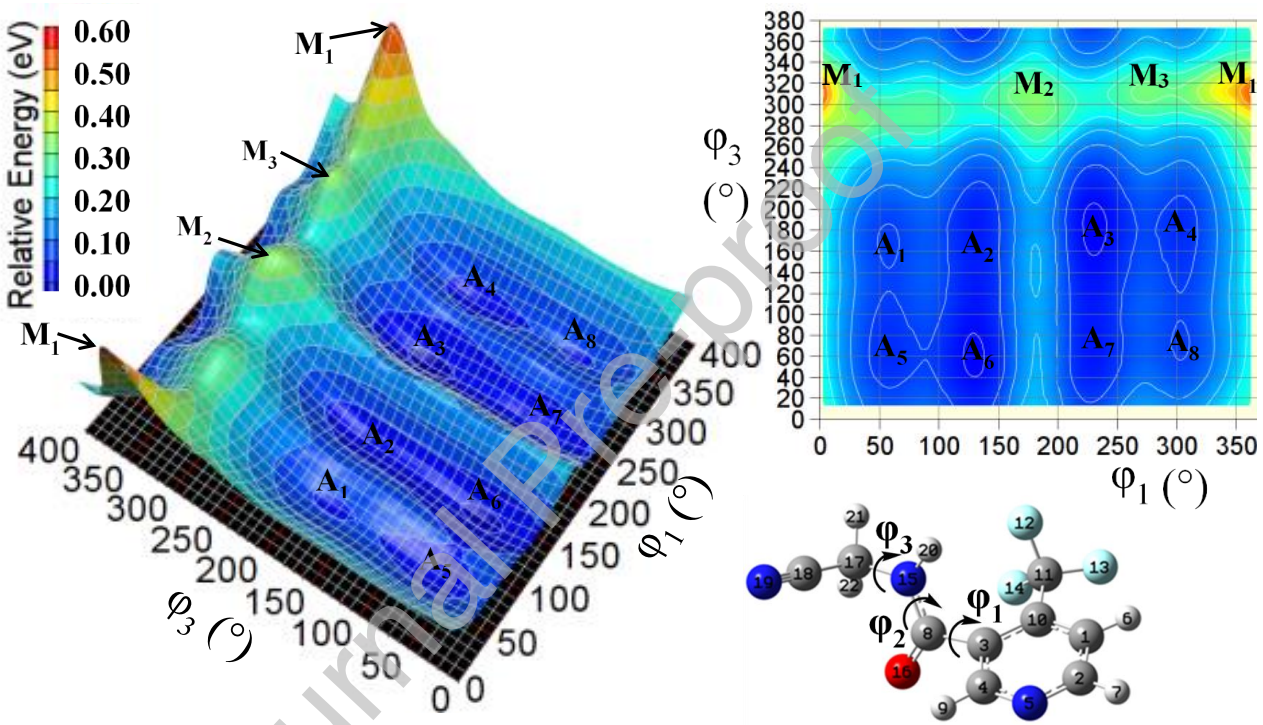

Figure 3. Potential energy surface (left) considering the scan around bonds N15–C17 and C3–C8, corresponding to φ_1 and φ_3 dihedral angles, respectively and its corresponding PES projection (right). Energy values are relative to the global minimum.

The additional energy observed in M_1 can be explained considering the electronic repulsion that is present when all the groups in the principal side chain ($–CF_3$, –C=O and –CN) adopted a disposition such as all of them pointed in the same direction (Fig. 2A). Another two maxima were found: M_2 corresponding to φ_1=182° and φ_3 =313° and M_3 with φ_1=272° and φ_3 =313°.

The different zones containing the minima follow the subsequent increasing order in energy: $A_6 < A_3 < A_2 < A_7 < A_5 < A_4 < A_8 < A_1$. The less energetic conformer was observed in the A_6 zone for a geometry with φ_1=122° and φ_3 =73° (Fig. 4). From a careful inspection of the geometries of each minima and a comparison between the eight most stable conformers obtained in gas phase (B3LYP/6-311+G(d,p)), we established correspondences as resumed in Table 2.

Table 2. Values for dihedral angles in different zones with minima of the PES.

PES Zone	Conformer B3LYP/6-311+G(d,p) in gas phase (from Table S1)	φ_1 (°)	φ_3 (°)	Relative Energy (eV)
A_1	**7**	49–70	140–190	0.046–0.057
A_2	**3**	100–150	130–220	0.013–0.056
A_3	**4**	220–240	155–210	0.003–0.030
A_4	**6**	280–320	120–230	0.035–0.059
A_5	**8**	40–80	30–120	0.033–0.053
A_6	**2**	130–140	40–80	0.000–0.042
A_7	**5**	210–250	15–140	0.020–0.045
A_8	**1**	290–310	55–95	0.045–0.052

Therefore, each conformer obtained with the methodology implemented in the conformational search (explained at the beginning of section 2.1) has its equivalent in one zone of the as-obtained surface for a simultaneous scan of φ_1 and φ_3. Therefore, it validates the proposed methodology for this study. The analysis for the interconversion between different geometries in the minima of the PES deserves special attention (Fig. 4).

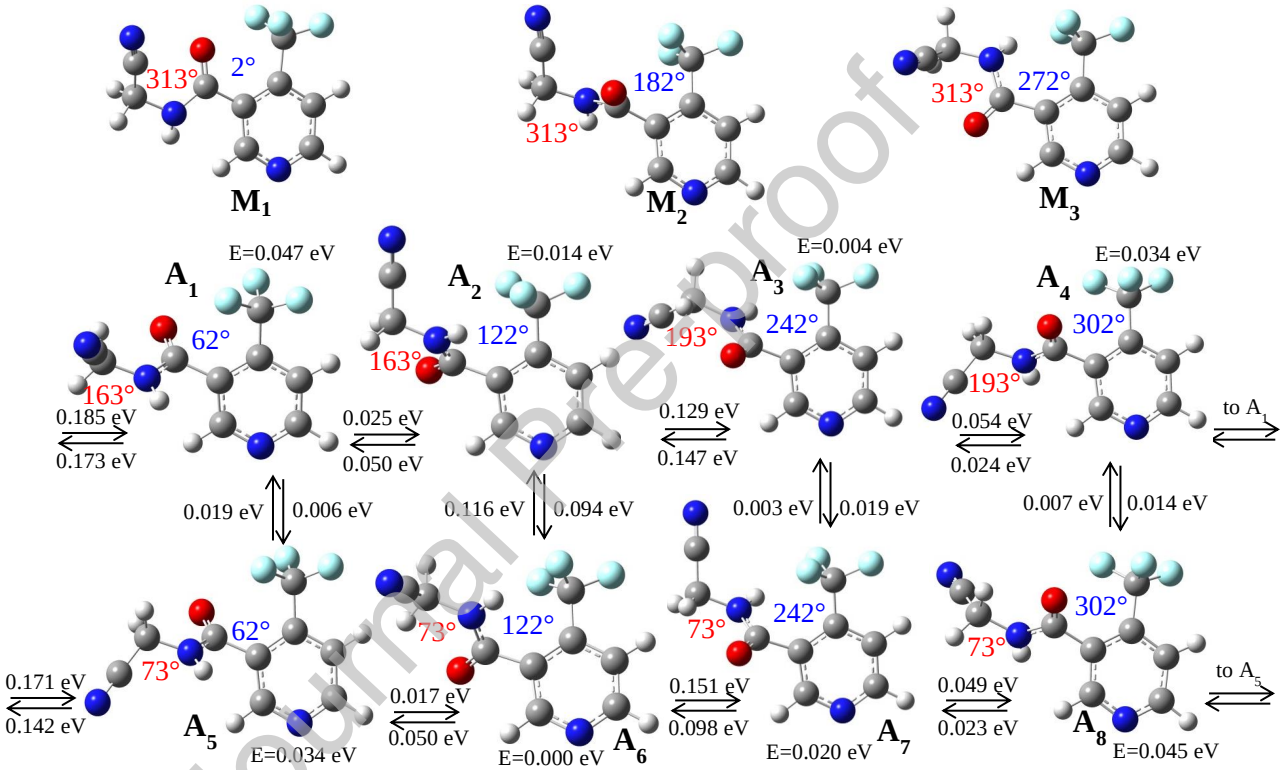

Figure 4. Maxima (up) and inter-conversion between minima (down) obtained from the PES. φ_1 (blue) and φ_3 (red) values.

Table 2 resumed the range for the dihedral angles in the different zones of the PES. Starting from the most stable conformer A_6, an anti-clockwise rotation of 60° in φ_1 conduces to A_5 with a barrier of 0.050 eV (1.15 kcal/mol) and 0.017 eV (0.39 kcal/mol) in the opposite direction (Fig. 4). Here, energy barriers are defined as the difference between a local minimum and the relevant highest energy point connecting two minima in the PES map.

On the other hand, a rotation of φ_1=120° (starting from A_6) produces A_7 with a barrier of 0.151 eV (0.35 kcal/mol) and 0.098 eV (2.26 kcal/mol) in the opposite direction (coming back from A_7 to A_6). Another rotation of φ_1=60° leads to A_8 and finally A_5 for a rotation of φ_1=120°. Respective barriers are resumed in Fig. 4. In this route, the value of φ_3 was kept at 73° while varying φ_1. Therefore, this scheme involves the gradual variation of one dihedral in 60° or 120°, alternatively, to produce the first series of minima: A_5, A_6, A_7 and A_8.

Another route connecting minima also involves rotations of 60° and 120° (alternatively) around φ_1. Two values are observed for φ_3: 163° and 193°. Therefore, this requires a further variation of two dihedrals at the same time for only once. This route connects A_1, A_2, A_3 and A_4 as can be seen in detail in Fig. 4. It produces the second series of minima.

Minima from the first and second series are interconnected by rotations of 90° and 120° in φ_3, while φ_1 is kept constant.

From the PES map, those conformations having a φ_3 value between 280° and 320° exhibited a high energy for any value of φ_1 as well as geometries with φ_1 in the range of 350° and 360°/0° for any φ_3 value. A torsional energy of 0.034 eV (0.79 kcal/mol) and 0.125 eV (2.89 kcal/mol) has been reported previously [47] for the C–C–C–O torsional angle in benzamide. This energy has been obtained starting from the synperiplanar

conformation (30°) of benzamide and moving to the *cis* (0°) and *orthogonal* (90°) forms, respectively. Therefore, energetic barriers found in this study are in good agreement with previous reports.

Moreover, for the eight most stable conformers, four of them maintain a relation of specular images with one of the conformers in other four zones. This situation was also reported in other studies. [49] The pair of zones for conformers that maintain a relation of mirror images are: A_2/A_7; A_1/A_8; A_4/A_5 and A_3/A_6. They can be converted between each other by properly rotations of φ_1 and φ_3 as is briefly analyzed in Section S2.

3.3.Vibrational spectroscopic analysis

Vibrational spectroscopy provides a potentially powerful technique for studying the conformational structure of organic molecules. However, it depends not only on obtaining IR and/or Raman spectra of such systems, but also on the ability to interpret these spectra in the greatest possible detail. This kind of analysis can succeed only if a secure predictive capability exists. In other words, experimental observations must be complemented by theoretical normal vibration calculations.

In that sense, density functional methods are increasingly used by spectroscopists for modeling molecular properties that include equilibrium structure, vibrational frequencies, and intensities. The title compound is constituted by 22 atoms and hence exhibits 60 normal modes of vibration. The observed and calculated wavenumbers and potential energy distributions are discussed below.

The experimental spectrum has been reported by Sahu et al. [14], therefore, we will not present the corresponding spectrum here in order to avoid repetitive information. Instead of,

the signals observed in the experimental spectra are compared with the calculated and properly scaled frequencies obtained by DFT methodology (Table 3). The calculated IR intensities of the final spectra were also scaled by the respective abundances of the individual conformers.

Some minor discrepancies between calculated (scaled) and observed frequencies may exist because experimentally FT-IR spectra of the solid sample was recorded in KBr disc. In that case, inter-molecular interactions are present and may be considered. For this reason, we performed calculations based on PCM using a relative permittivity of the solvent continuum (ε_r) of 78.39 for water, to obtain a more realistic model.

The title compound consists of a nicotinamide substituted by trifluoromethyl group in the pyridine ring and a cyanomethyl group bounded to the carboxamide group. Hence, the vibrational modes are discussed under five heads: (i) amide group vibrations, (ii) pyridine ring vibrations (iii) trifluoromethyl group vibrations, (iv) CH_2 group vibrations and (v) cyano group vibrations. Stretching vibration (ν), in–plane bending (β), out of plane bending (γ), torsion in–plane (τ) and torsion out of plane (τ_{oop}) modes, respectively, were resumed in Table 3.

Table 3. Comparison of experimental infrared wave numbers (cm^{-1}) with theoretical harmonic frequencies (cm^{-1}) of flonicamid, scaled by 0.944 factor at the M06-2X/6-311+G(d,p) level of theory for the most stable conformer in solvent (water).

Experimental	Calculated scaled		Description of dominant modes in order of decreasing Potential energy distribution (PED > 10%)
wavenumbers	Frequencies	Intensities	
3281 (m)	3449	39.44	ν NH (100)
3062 (vw)	3067	0.87	ν CH aromatic (97)
	3032	8.22	ν CH aromatic (95)
3006 (vw)	3022	11.86	ν CH aromatic (95)
2920 (w)	2993	11.14	ν as CH_2 (99)
	2937	17.34	ν CH_2 (84)
2250 (vw)	2282	4.16	ν $C^{18}N^{19}$ (91)
1654 (vs)	1660	276.81	ν CO (86) (amide I)
1574 (m)	1579	15.92	ν ring mode 8a (61)
	1555	15.99	ν ring mode 8b (41) + β scissoring $C^3C^4N^5$ (17)
1538 (st)	1476	214.86	β scissoring $H^{20}N^{15}C^{17}$ (44) + ν $N^{15}C^{17}$ (17) (amide II)
1498 (w)	1456	63.41	ν ring mode 19a (54) + β scissoring $H^{20}N^{15}C^{17}$ (16)
1406 (m)	1374	18.51	β (scissoring) CH_2 (85)
1356 (w)	1369	22.41	ν ring mode 19b (67)
1324 (vs)	1314	8.13	γ (wagging) CH_2 (67)
1290 (st)	1274	52.49	β CH mode 3 (46)
	1268	218.12	ν CCF_3 (21) + β CH mode 18a (18) + ν as CC and CN ring (14)
1237 (st)	1242	105.13	ν ring mode 14 (29) + γ (twisting) CH_2 (11)
1195 (vs)	1222	52.49	γ (twisting) CH_2 (37)+ ν ring CC and CN (35)
	1200	55.96	β $H^{20}N^{15}C^{17}$ (21) + ν ring CC and CN (15) + ν C^3C^8 (-11) + ν as $C^{17}N^{15}C^8$ (10) (amide III)
1168 (vs)	1158	21.13	β ring mode 9a (44) + β $H^7C^2N^5$ (15)
1134 (vs)	1136	90.31	β ring mode 18b (17) + ν as $C^{17}N^{15}C^8$ (39)
	1127	226.72	ν as CF_3 (77) + β FCF (10)

	1101	201.01	ν as CF_3 (60) + β FCF (11)
1067 (s)	1045	34.60	ν ring CC and CN (42) + β $H^6C^1C^2$ (13)
1030 (s)	1032	66.46	ν $C^8N^{15}C^{17}$ (-21) + ν s CF_3 (-19) + β ring (scissoring) (15)
1005 (ssh)	1018	11.96	ν $C^8N^{15}C^{17}$ (17) + ν ring mode 1 (12) + β (scissoring) $C^{17}C^{18}H^{21}$ (10)
	969	1.35	τ $H^7C^2N^5C^4$ (58)
	953	12.65	τ oop ring (40) + γ (twisting) CH_2 (20)
911 (m)	918	0.54	τ $H^9C^4N^5C^2$ (70)
	869	13.15	ν $C^{17}C^{18}$ (48) + τ CH_2 (29)
843 (m)	824	34.21	τ oop ring (wagging) (71)
794 (m)	799	7.95	β C^3C^8 $O^{16}N^{15}$ (30) + ν C^3C^8 (11)
	763	5.10	τ ring mode 4 (65)
746 (w)	753	0.56	ν CF_3 (31) + β ring mode 4 (21)
709 (m)	723	1.31	τ oop ring (40) + γ $O^{16}C^3N^{15}C^8$ (amide V) (10)
663 (vs)	682	3.83	β ring mode 6b (27) + β $O^{16}C^8N^{15}$ (amide IV) (10)
	633	30.30	β ring mode 6a (67)
	593	7.36	τ ring (30) + τ oop $C^4C^3C^8O^{16}$ (12)
	585	9.49	τ ring (14) + β $N^{15}C^{17}C^{18}$ (12)
	566	1.82	β as CF_3 (39)
	513	3.70	τ ring (16) + β FCF (13) + β $N^{15}C^{17}C^{18}$ (10)
	473	3.91	β as FCF (42) + τ $C^{20}C^{15}C^8C^3$ (10)
	451	57.83	τ $H^{20}N^{15}C^8C^3$ (72)
	398	5.58	β FCF (66)
	360	9.65	τ ring mode 16b (22) + ν $C^{10}C^{11}$ (13)
	353	0.72	β $C^{17}C^{18}N^{19}$ (63) + τ oop ring (25)
	336	9.30	τ ring mode 16a (39)
	305	17.10	β $C^8N^{15}C^{17}$ (20) + β $C^{10}C^{11}F^{12}$ (12)
	281	1.05	β rock CF_3 (26) + β C–CONR (20)
	254	0.55	τ oop ring (17) + τ $C^8N^{15}C^{17}C^{18}$ (15)
	240	15.05	γ C–CONR (27) + β $C^8N^{15}C^{17}$ (13) + β rock CF_3 (13)

203	0.17	β $C^{1}C^{10}C^{11}$ (15) + β $C^{3}C^{10}C^{11}$ (14)
135	8.40	τ ring (44)
115	0.22	τ oop ring (29) + β $F^{12}C^{11}C^{10}C^{1}$ (11)
92	5.52	τ ring (32)
73	5.01	τ ring (48) + τ $C^{18}C^{17}N^{15}C^{8}$ (20)
61	1.78	τ $C^{17}N^{15}C^{8}O^{16}$ (79) + τ $C^{18}C^{17}N^{15}C^{8}$ (10)
40	5.54	τ oop $O^{16}C^{8}C^{3}C^{10}$ (18) + τ oop $H^{21}C^{17}N^{15}C^{20}$ (11)
33	2.47	τ CH_2 (42)

vs: very strong; st: strong; w: weak; vw: very weak; ν: stretching; s: symmetric; as: asymmetric; β: in-plane bending; γ: out of plane bending; τ: in-plane torsion; τ oop: out of plane torsion. PED less than 10 % is not shown.

3.3.1. Amide group vibrations

The characteristics absorption bands corresponding to the amide are due to the stretching vibrations of the N–H and C=O groups, NH deformations and to mixed vibrations known as "amide bands". [50] The band in the range 3220–3140 cm^{-1} in secondary amides was assigned to the associated N–H stretching of a *cis*–bonded complex while a band in the range 3340–3270 cm^{-1} was assigned to a *trans*–bonded structure. In this study, the N–H stretching frequency in the experimental spectra was observed as an absorption band of middle intensity at 3281 cm^{-1} while the theoretical predicted value was found at 3449 cm^{-1}. A possible explanation for this difference may be that PCM consider infinite dilute solutions. Thus, the calculated frequency is in good agreement with experimental values expected for a free N–H stretching band of secondary amides in the range 3470–3400 cm^{-1} in dilute solutions. [50]

On the other hand, the C=O stretching (known as amide I band) was evidenced as an extraordinarily strong band at 1654 cm^{-1} in the experimental spectra which agrees with the calculated value of 1660 cm^{-1}. In general, this band is present at 1670–1630 cm^{-1} and 1670–1630 cm^{-1} for secondary amides in solid and diluted solutions, respectively. Furthermore, the amide II band in this kind of amide appears due to a mixed vibration involving the N–H in–plane bending (β) and the C–N stretching vibration. This band was observed at 1538 cm^{-1} in the experimental spectra and at 1476 cm^{-1} in the calculated one. There are reports [51] indicating that the state of the secondary amide affects the location of this band, therefore, this effect can explain the differences between the experimental and calculated frequencies.

The amide III band was evidenced at 1195 cm^{-1} in the experimental spectrum and at 1200 cm^{-1} in the calculated one. This band appears due to a characteristic mixed vibration involving the C–N stretching and N–H bending but in the studied molecule it also exhibited mixing with other vibrations modes.

The amide IV band is characteristic of secondary amides, which is due mainly to the O=C–N bending and was observed at 663 cm^{-1} in the experimental spectra and at 682 cm^{-1} in the calculated one. On the other hand, the amide V band of secondary amides appears near 700 cm^{-1} and is characteristic of the N–H out of plane deformation. The last one was evidenced at 709 cm^{-1} and 723 cm^{-1} for the experimental and theoretical spectrum, respectively.

3.3.2. 3,4–disubstituted pyridine vibrations

Three bands corresponding to the C–H stretching of the di–substituted pyridine were found at 3067 cm^{-1}, 3032 cm^{-1} and 3022 cm^{-1} in the calculated spectra. These bands agree well with a very weak signal found at 3062 cm^{-1} in the experimental spectra.

In reference to the CC and CN ring stretching vibrations, it has been established [52] that the intensities of the bands in the 1620–1400 cm^{-1} region, for the substituted pyridines depend upon the electronic nature of the substituent, whereas the positions of the bands are relatively invariant. In this paper, we followed Wilson's notation for the benzene ring modes [53], known as C–C stretching vibrations in benzene and its derivatives. Flonicamid molecule contains a Nitrogen and five Carbon atoms in its aromatic ring, therefore four C–C and two C–N stretching vibrations were obtained. The modes 8a, 14, 19a and 19b correspond to the C–C stretching vibrations, whereas the modes 1 and 8b represent C–N stretching vibrations. Modes 8a and 8b are observed at 1579 and 1555 cm^{-1}, respectively, in

agreement with previous results obtained for a 3,4-disubstituted pyridine ring. [54] The higher frequency has about 61 % C–C stretching character while the lower frequency mixes a 41 % of the C–N stretching mode with $C^3C^4N^5$ bending in–plane vibration. On the other hand, modes 19a and 19b are expected in the 1400–1500 cm^{-1} spectral range for benzene and its derivatives. In analogy, flonicamid molecule exhibits a higher frequency (1456 cm^{-1}) due to a C–C stretching mode to the extent of 54 % with a certain amount of mixing with $H^{20}N^{15}C^{17}$ in–plane bending vibration, whereas the lower frequency (1369 cm^{-1}) has C–C stretching character to the extent of 67 % PED.

Modes 1, 6a and 6b in benzene were refereed to vibrations of the aromatic nucleus and were found to be sensitive to the position and nature of the substituent in substituted pyridine rings. [54] In benzene, a signal at 990 cm^{-1} has been adjudicated to mode 1 of ring vibration mode which consists in a pure C–C stretching vibration, totally symmetric and widely separated from C–H stretching modes. This mode has been found at 1018 cm^{-1} in the calculated spectra of flonicamid, which mixes with other modes. On the other hand, mode 6a and 6b were found at 633 cm^{-1} and 669 cm^{-1}, respectively. The first one mixes with umbrella vibration mode of trifluoromethyl group while the second one mixes with amide IV band.

Mode 14 was evidenced at 1237 cm^{-1} and 1242 cm^{-1} in experimental and calculated spectra, respectively, and corresponds to Kekule's mode in which alternate C–C bonds either increase or decrease. It exhibits certain mixing with twisting of the methylene group.

On the other hand, ring torsions were designated as modes 4, 16a and 16b in benzene and its derivatives. In the studied molecule, mode 4 was evidenced at 763 cm^{-1} in which CCCC

torsion angles either increase or decrease and presented a 65 % PED. In mode 16a, these angles change in the ratio +2, -1, -1, +2, -1, -1, whereas in mode 16b, they change in the ratio 0, +2, -2, 0, +2, -2, as reported by Laxman Naik et al. [54] Therefore, mode 16a and 16b were found mixed with other modes at 336 cm^{-1} and 360 cm^{-1} in the calculated spectra, respectively.

In-plane ring bending was assigned to mode 3 which was found at 1274 cm^{-1} and 1290 cm^{-1} in calculated and experimental spectra, respectively, having a 46 % PED due to C–H in–plane bending character. Laxman Naik et al. [54] reported three other C–H in–plane bending vibrations, designated as mode 9a, 18a and 18b in di-substituted pyridine rings. In aromatic compounds, these modes generally appear in the 1000–1200 cm^{-1} spectral region. Therefore, the bands near 1158 cm^{-1}, 1268 cm^{-1} and 1136 cm^{-1} are assigned as 9a, 18a and 18b modes, respectively.

Another type of vibration is related with the bond between pyridine ring and the principal side chain. Laxman Naik et al. proposed that modes 7b and 13, found at 1072 cm^{-1} and 1305 cm^{-1}, represent the C–C^{α} stretching vibrations in a 3,4–disubstituted pyridine. Moreover, Velcheva et al. [8] reported a C–$CONH_2$ stretching frequency at 790 cm^{-1} in nicotinamide. Therefore, frequencies observed at 1200 cm^{-1} and 799 cm^{-1} correspond to C^3–C^8 stretching, which are mixed with other modes in the calculated spectra of flonicamid. On the other hand, in–plane bending of the C–CONR group was found at 281 cm^{-1} and out of plane bending at 240 cm^{-1}.

3.3.3. Trifluoromethyl group vibrations

It has been suggested that for all the benzene derivatives containing trifluoromethyl groups, a broad band near 1330 cm^{-1} appears as very intense band in the IR spectrum. [55] Thus, the signal at 1268 cm^{-1} in the calculated spectra evidenced a character of 21 % of C–CF_3 stretching mixed with other modes. On the other hand, two different CF_3 asymmetric stretching mode has been reported at 1200 cm^{-1} and 1197 cm^{-1} [55] in benzene derivatives, in the present paper the mentioned mode was found at 1127 cm^{-1} and 1101 cm^{-1}. Furthermore, CF_3 symmetric stretching mode was found at 746 cm^{-1} and 753 cm^{-1} in experimental and calculated spectra, respectively, which agrees with the previous frequency at 740–780 cm^{-1} reported by some authors [55, 56]. Asymmetric deformations of CF_3 group were found at 566 cm^{-1} and 473 cm^{-1}, while the symmetric mode was observed at 398 cm^{-1}. On the other hand, CF_3 rocking was present at 281 cm^{-1} and 240 cm^{-1}, while torsion vibration was evidenced at 115 cm^{-1}, all of them in good agreement with results reported previously. [55, 57]

3.3.4. CH_2 group vibrations

The CH_2 asymmetric and symmetric stretching modes have been evidenced in the calculated spectra at 2993 cm^{-1} and 2937 cm^{-1}, respectively. These modes are also observed as a weak signal in the experimental spectra at 2920 cm^{-1}. The four bending vibrations of methylene group: scissoring, wagging, rocking, and twisting are evidenced in the calculated spectra at 1374 cm^{-1}, 1314 cm^{-1}, 1222 cm^{-1} and 953 cm^{-1}, respectively.

3.3.5. Cyano group vibrations

The C–N stretching of cyano group was evidenced at 2250 cm^{-1} and 2282 cm^{-1} in the experimental and calculated spectrum, respectively. Those values are consistent with

previous reported frequencies in several nitrile molecules. [58] On the other hand, the bending mode associated with the C–C≡N skeleton was observed at 353 cm^{-1} which agrees with previous results reported for substituted nitriles. [58]

3.4.Frontier Molecular Orbitals (FMO) and UV/Vis spectra

Studying the electronic structure by UV spectral and quantum chemical methods is important, not only for interpretation of the spectra, but also to estimate the direction of the electronic density redistribution of the compounds, which is a determining factor of their reactivity and biological activity. The highest occupied molecular orbital (HOMO) and the lowest unoccupied molecular orbital (LUMO) are named as Frontier Molecular Orbitals (FMO). The gap between these orbitals supports a description of the chemical reactivity and the kinetic stability of the molecule. A molecule having a small frontier orbital gap is generally associated with a high chemical reactivity, low kinetic stability and is also treated as a soft molecule. [59]

The distributions of the HOMO and LUMO orbitals computed by time dependent DFT (TD-DFT) at the B3LYP/6-311+G(d,p)/PCM(water) level for the title molecule are illustrated in Fig. 5. The calculated energy values are $E_{HOMO} = -2.54$ eV and $E_{LUMO} = -7.93$ eV. The results indicate that the studied compound exhibit 58 occupied molecular orbitals (MOs). Both frontiers' orbitals exhibit approximately the same delocalization around the whole molecule. The title molecule has a relative high HOMO–LUMO gap of 5.40 eV, which may imply high kinetic stability and low chemical reactivity. [60, 61]

The calculated electronic absorption spectrum as well as the vertical excitation energies and oscillator strengths are shown in Fig. S7. It exhibits an intense peak between 140–200 nm, centered at 176 nm and a less intense broad band between 210–300 nm, centered at 248 nm.

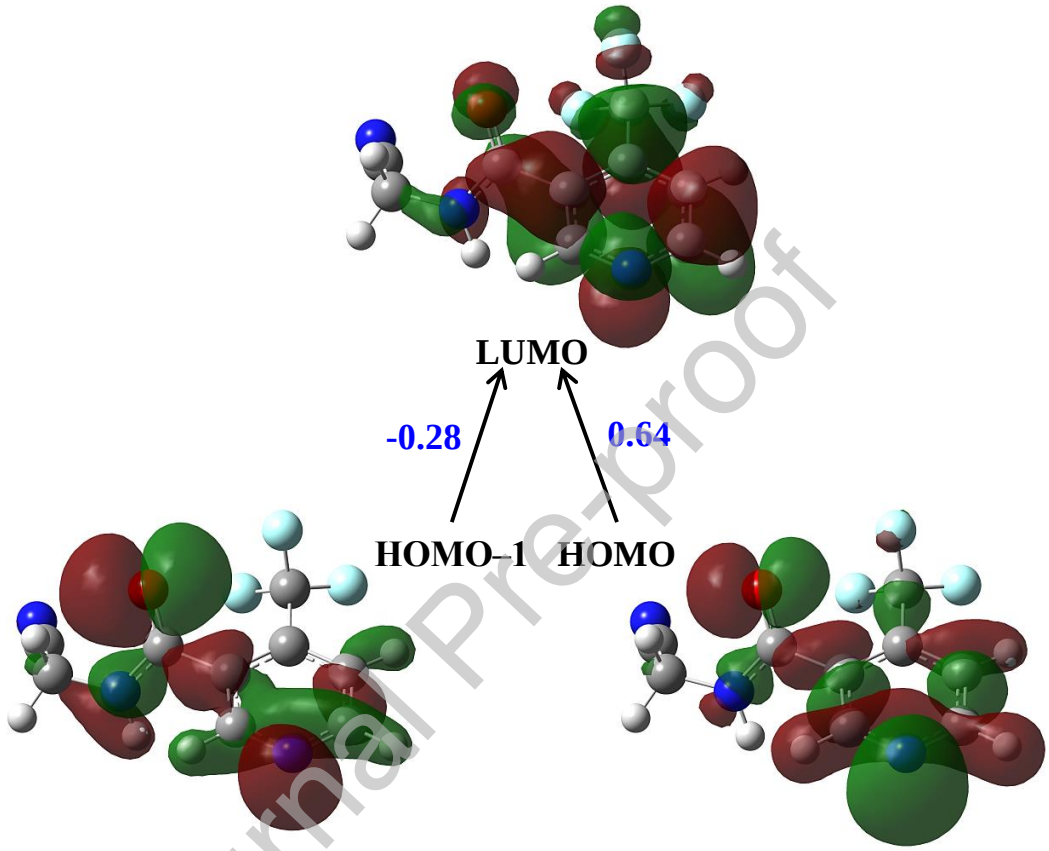

Figure 5. Schematic diagram of MOs and transitions (each labeled with the corresponding coefficient) for the first excited state in the title compound.

Therefore, flonicamid exhibit absorption in the UV spectral region. The first excited state is appreciated at 281 nm, related with the energy of 4.41 eV due to the electronic transitions in the following orbitals: 57→59 and 58→59, which correspond to HOMO–1→LUMO and HOMO→LUMO, respectively. Moreover, we found that a 90.7 % of the transition for the first excited state is due to the electron density moving from HOMO to LUMO with a small

contribution of 9.3 % from HOMO–1 to LUMO. As can be seen in Fig. 5, it is evident that this transition corresponds to n→π* with the electron density moving from the principal chain of the molecule (which contains the most important functional groups) to the region of the pyridine ring and its trifluoromethyl group. The excitation energies, oscillator strengths, and contributing configurations for fifty excited states of flonicamid were collected in Table S2.

3.5.Molecular electrostatic potential (MEP)

MEP is related to the electronic density and is a useful descriptor in understanding sites for electrophilic and nucleophilic reactions as well as hydrogen bonding interactions. The value of the molecular electrostatic potential, *V(r)*, for a molecular system at a point gives the electrostatic energy on the unit positive charge located at the distance *r*. The electrostatic potential *V(r)* is also well-established as a guide to molecular reactive behavior and for analyzing processes based on the "recognition" of one molecule by another, as in drug-receptor, and enzyme-substrate interactions. [62] The *V(r)* values can be determined experimentally by X-ray diffraction or by computational methods. [63, 64] In the present study, the MEP and a two dimensional (2D) contour map drawn in the molecular plane clearly suggest different values of electrostatic potential in the molecule (Fig. 6).

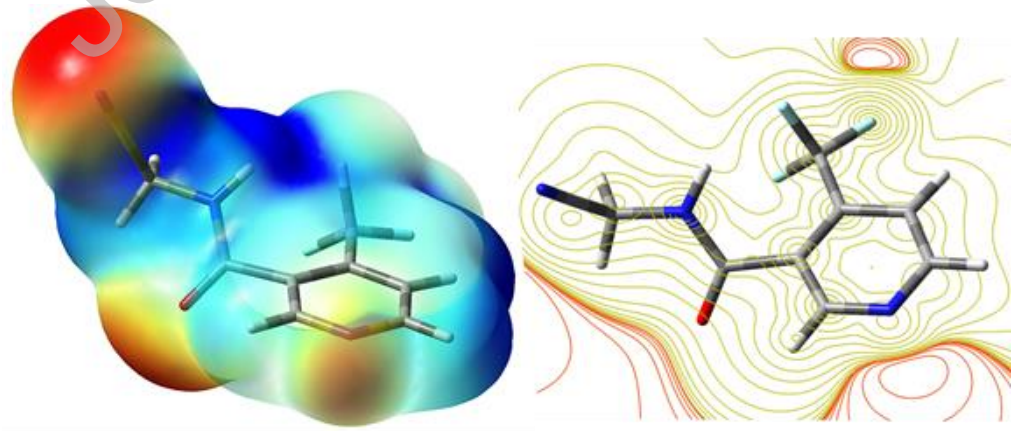

Figure 6. MEP and 2D contour map of the title compound. The maximum positive regions which are preferred sites for a nucleophilic attack are shown in blue; the maximum negative regions which are preferred sites for an electrophilic attack are shown in red.

Negative regions associated with N5, O16 and N19 suggested that these are the most preferred regions for electrophilic attack. On the other hand, the most positive regions are localized on the following hydrogen atoms: H6, H7, H20, H21 and H22, therefore one can predict that these are preferred site for a nucleophilic attack. We will demonstrate that these active regions in the molecule are uniformly supported by other reactivity descriptors like Fukui functions, dual descriptor and their corresponding condensed versions and sustained the molecular interaction of flonicamid with biological targets, as will be explained in the following sections.

3.6.Fukui functions and dual descriptor

The chemical reactivity is often studied by using the Fukui functions [65] and the dual descriptor ($\Delta f(\boldsymbol{r})$). If $\Delta f(\boldsymbol{r}) > 0$, then the site is favored for a nucleophilic attack, whereas if $\Delta f(\boldsymbol{r}) < 0$, then the site could hardly be susceptible to undertake a nucleophilic attack, but it may be favored for an electrophilic attack. Readers are referred to section S5 for a theoretical background.

Often, one prefers to associate molecular properties like chemical reactivity with atomic entities in the molecule and not with a certain point in space. This means one needs to somehow identify an atom in the molecule. In that sense, Fukui functions are often condensed to atomic resolution. The Fukui functions f_k^+ and f_k^- describe the ability of an

atom "*k*" to accommodate an extra electron or to cope with the loss of an electron. On the other hand, f_k^0 is then considered as an indicator for radical reactivity.

Therefore, seeking to unambiguously identify the reactivity behavior of the considered molecule, we studied the $f^+(\boldsymbol{r}), f^-(\boldsymbol{r}), f^0(\boldsymbol{r})$ and $\Delta f(\boldsymbol{r})$ global descriptors. These are represented in Fig. 9 and we have chosen to display in purple the zone with $\Delta f(\boldsymbol{r}) > 0$ and in yellow the areas with $\Delta f(\boldsymbol{r}) < 0$. Thus, Fig. 7 represents a map of the nucleophilic/electrophilic behavior of the different sites within the molecule.

We evidenced that region where $f^-(\boldsymbol{r}) > 0$ and $\Delta f(\boldsymbol{r}) < 0$ are predominant around N5 and O16, which clearly indicate the nucleophilic character of the zones due to its rich electron density and consequently, attracting to electrophiles. Small purple and yellow lobes related with $f^-(\boldsymbol{r})$ and $\Delta f(\boldsymbol{r})$, respectively, are also present in N15, N19 and in the pyridine ring, principally at positions adjacent to N5 (C2 and C4) in the aromatic ring.

On the other hand, region having $f^+(\boldsymbol{r}) > 0$ and $\Delta f(\boldsymbol{r}) > 0$ are considered as electrophilic centers and are represented as purple lobes in the respective diagrams (Fig. 7). The purple lobes are principally located along the aromatic ring, which was expected having in mind that pyridine should be considered as a deactivated ring to electrophilic aromatic substitution, even more, if one considers the presence of the electron withdrawing trifluoromethyl group. Therefore, having in mind this behavior and considering that the $-CF_3$ group attracts electron density from C10, we propose that flonicamid's ring may exhibit the classical behavior of an activated ring (as for some pyridines) in a nucleophilic aromatic substitution. On the other hand, it should exhibit the corresponding behavior in electrophilic aromatic substitutions.

On the other hand, the $f^0(\boldsymbol{r})$ identifies some zones primarily located close to the pyridine ring and O16 and are supported by condensed Fukui functions and condensed dual descriptors as can be seen from Fig. 7 and Table S3.

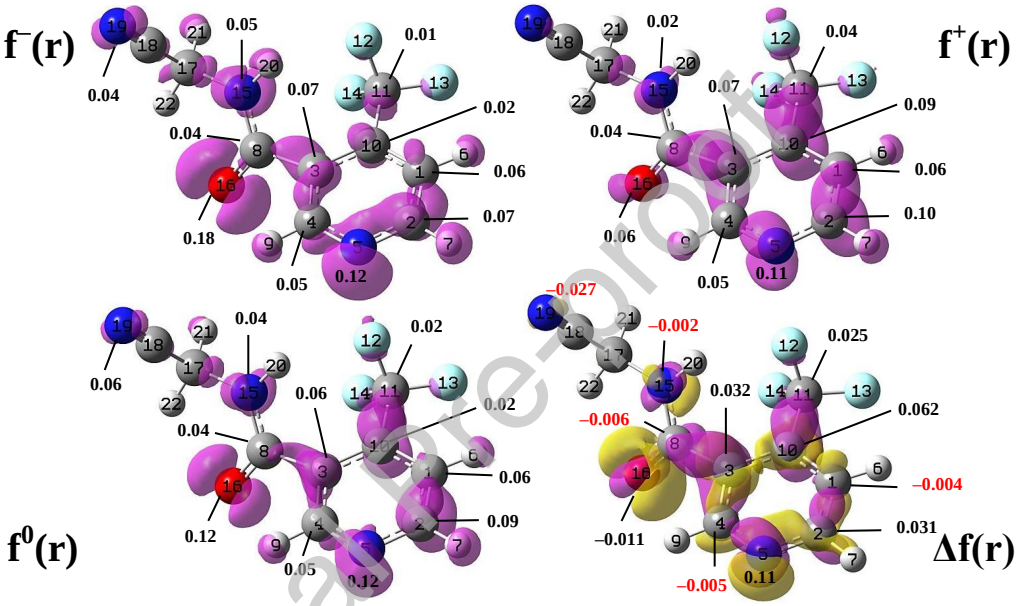

Figure 7. Isosurfaces of the Fukui functions ($f^+(\mathbf{r})$, $f^-(\mathbf{r})$, $f^0(\mathbf{r})$) and dual descriptor ($\Delta f(\mathbf{r})$) for the most stable conformer of flonicamid in gas phase. Fukui functions are monophasic functions (purple-colored lobes only), being positive and reveal site of electrophilic, nucleophilic, and radical behavior, respectively. Dual descriptor is a biphasic function, so that purple-colored lobes indicate electrophilic behavior, denoting $\Delta f(\mathbf{r}) > 0$, meanwhile yellow-colored lobes reveal nucleophilic behavior, associated to $\Delta f(\mathbf{r}) < 0$. All isosurfaces were generated at a 0.003 a.u. at the B3LYP/6-31G(d) level of theory. The numbers represent condensed Fukui functions and condensed dual descriptors.

The obtained results for condensed Fukui functions and condensed dual descriptors are shown as numbers for selected atoms in Fig. 7. A complete list of the condensed Fukui functions and condensed dual descriptors is also presented in Table S3 as electronic supplementary information associated to this paper. From the calculated values, the reactivity order for the electrophilic attack is N5 > C2 > N19 > C1 > C4 > N15 > H7 > C8 > C3 > H6 > C10 > H9 > H21 > H20 > F13 > F12 > C17 > F14 > C18 > H22 > C11.

On the other hand, for the nucleophilic attack, the order is C2 > C10 > C3 > O16 > H7 > C1 > C4 > N19 > F12 > H6 > H9 > C8 > C11 > F14 > F13 > H21 > N15 > C17 > H22 > H20 > C18.

Positions of reactive electrophilic and nucleophilic sites are in accordance with the chemical behavior and are consistent with regions of the molecular electrostatic potential and the analysis considering $f^{+}(\boldsymbol{r})$, $f^{-}(\boldsymbol{r})$ and $f^{0}(\boldsymbol{r})$.

3.7.Docking study

3.7.1. Selection of conformers

Frequency (number in cluster) vs. Gibbs free energy of conformers were first plotted for each compound with the specific target DNA sequence (Fig. 8). Then, the best conformation interaction for each ligand with DNA sequence was selected considering the following criteria: clusters with highest frequencies, clusters with lowest Gibbs free energies (Table 4). From the histogram data, the clusters with the lowest energy conformers and the clusters with the highest frequency conformers do not always coincide. Different studies revealed that most probable conformations (belonging to the most populated cluster), generally correspond to the conformations that are experimentally observed in the

ligand-macromolecule complexes. This is due to the lack of precision in the calculation of interaction energy between the ligand and the macromolecule.

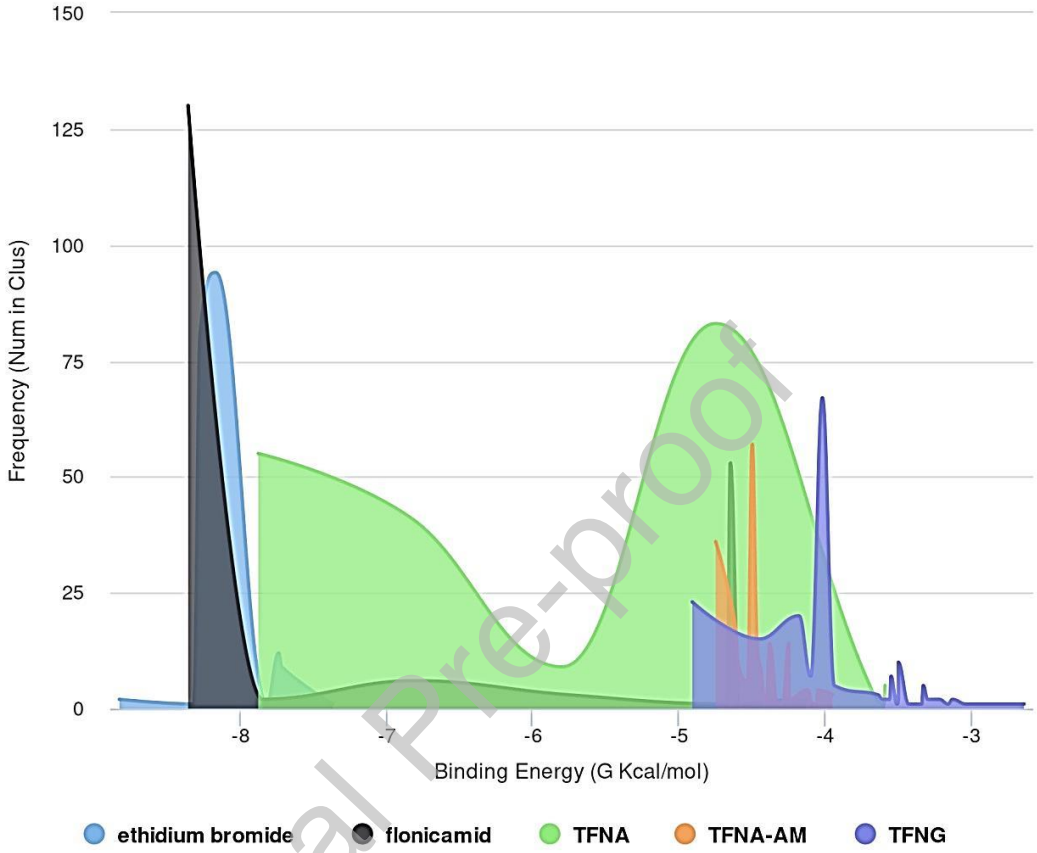

Figure 8. Cluster analysis of conformations. Frequency (number of conformers in clusters) of each compound after 200 runs considering the binding energy of conformations corresponding to the docking of flonicamid, TFNG, TFNA, TFNA-AM and ethidium bromide with DNA sequence 1BNA (interactive figure has been included as electronic supporting information).

The implemented force fields estimate the free energy using a single conformation of the macromolecule-ligand complex, so that the conformational entropy of the system is considered.

Finally, different studies indicated that the most populated clusters are those with favorable entropy for the formation of the macromolecule-ligand complex. Consequently, the conformations adopted in said clusters coincide with the binding modes observed experimentally in most cases. [45, 46, 66-68]

Flonicamid, TFNA, TFNA-AM and TFNG showed 9, 7, 19 and 28 clusters respectively on other hand ethidium bromide showed 8 clusters. Both flonicamid, TFNA and ethidium bromide showed a similar conformational dispersion, given by the clusters number, and similar affinities for the 1BNA sequence. Finally, TFNG and TFNA-AM also showed favorable binding energies for interaction with the 1BNA sequence but with lower affinities (Fig. 8 and Table 4). The chemical structure of three main metabolites of flonicamid are presented in Fig. S8.

Table 4. Lowest and Mean binding energy (ΔG, in kcal/mol), number of selected cluster and corresponding frequency calculated for the interaction between DNA sequence 1BNA and different ligands.

Compound	Lowest binding energy (ΔG kcal/mol)	Mean binding energy (ΔG kcal/mol)	Number in cluster (Frequency)	Conformation-interaction cluster n°
Flonicamid	-8.36	-8.35	130	1
TFNG	-4.02	-3.65	67	6
TFNA	-7.88	-7.87	55	1
TFNA-AM	-4.50	-4.38	57	5
Ethidium bromide*	-8.17	-8.06	94	4

* DNA intercalant compound control

3.7.2. Analysis and discussion of the molecular interactions

All the tested compounds bounded to the 1BNA DNA sequence. Fig. 9 shows the specific sites where the compounds flonicamid, ethidium bromide and TFNA are binding, which showed the best affinities for the selected DNA sequence.

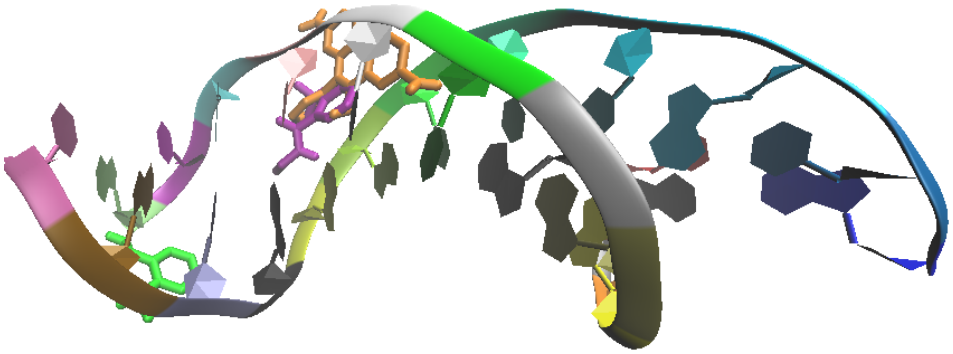

Figure 9. Three-dimensional (3D) molecular interaction of the compounds: flonicamid (purple), ethidium bromide (orange) and TNFA (green) with DNA sequence 1BNA.

Flonicamid interacts through 6 hydrogen bonds with residues: guanine10 (2.91Å), citosine9 (3.00Å), guanine16 (2.99Å), adenine17 (2.15Å) and adenine18 (2.33 and 3.10Å) (Fig. 10a). At this point, it is important to note that sites from the molecule related with these interactions are those observed in the Molecular Electrostatic Potential, analyzed previously in the section 3.5. On the other side, ethidium bromide interacts through 3 hydrogen bonds with residues: adenine18 (2.07Å), timine19 (3.05Å) and timine7 (2.15Å). It also showed a strong electrostatic interaction of the quaternary nitrogen attached to the ethyl group with the phosphate group of thymine20. Moreover, it exhibited hydrophobic interactions with other two DNA residues, adenine17 and citosine9 (Fig. 10b).

Flonicamid was classified as an agent for whom the weight of evidence is suggestive of carcinogenicity by various reports. [14, 69] In this study we are able to demonstrate that flonicamid binds with a similar affinity to that of the intercalating control compound ethidium bromide (-8.36 and -8.17 kcal/mol respectively). It also binds to the same region of the DNA 1BNA sequence (Fig. 10).

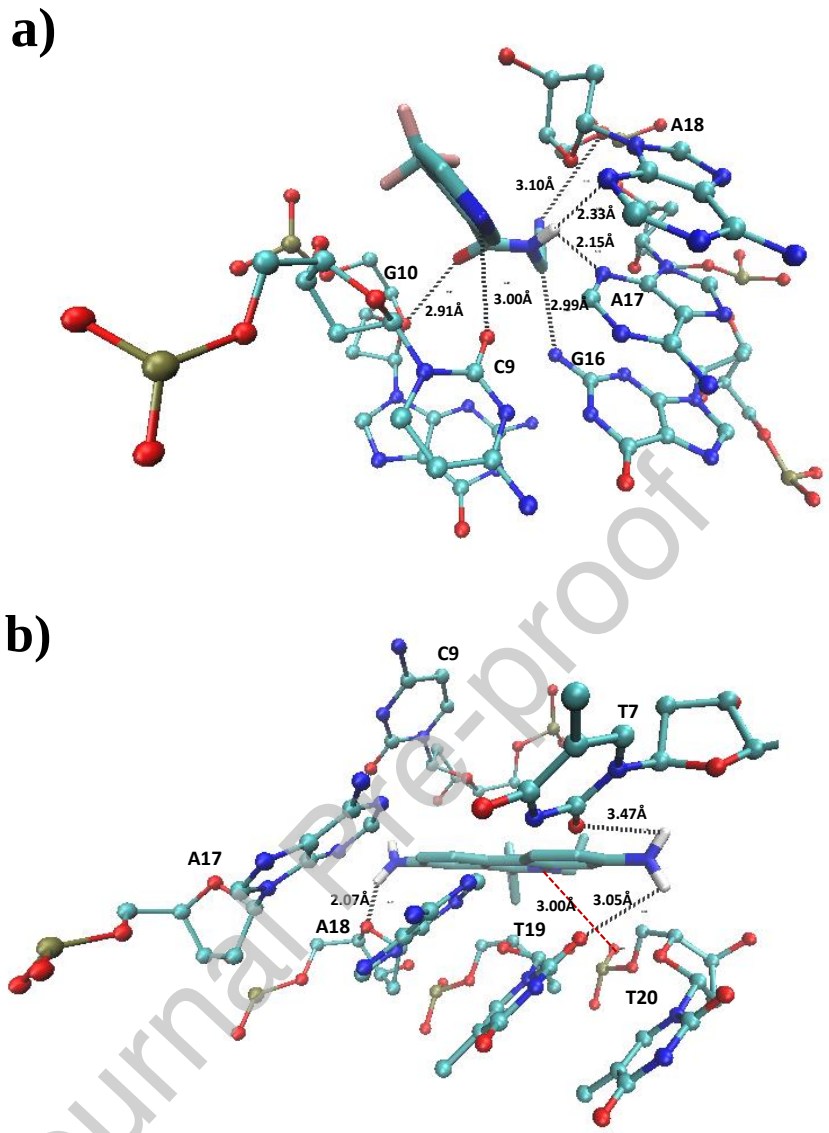

Figure 10. Three-dimensional (3D) molecular interaction of compounds: a) flonicamid and b) ethidium bromide with the DNA 1BNA sequence. Atoms: C (light blue), O (red), N (blue); H (white) and P (brown). The black dotted lines indicated Hydrogen bond and the red dotted lines indicated electrostatic interactions. Residues: A (adenine), T (timine), G (guanine) and C (citosine).

On the other hand, the TNFA metabolite (–7.88 kcal/mol) binds in a region of DNA close to flonicamid and ethidium bromide. The compound flonicamid and its TNFA metabolite

are the most worrying in terms of the high binding energies that they present. Despite this, the other two metabolites, TFNG and TFNA-AM, also demonstrated a certain affinity to the 1BNA sequence. The dissipation behaviors and the terminal residues of flonicamid and its metabolites in some crops and soils remain unclear.

The presence of flonicamid and its metabolites varies according to the crop and climatic conditions, for example a half-life time of 2 – 7 days was established for flonicamid and its metabolites in cabbage crops. [19] In another study it was shown that the risk, in the case of TFNG and flonicamid, was especially high, indicating that there is a certain intake risk of flonicamid in tea for human consumption. [16] The large-scale use would generate its accumulation and its possible effects as carcinogenic agents in humans are yet unknown.

4. CONCLUSIONS

Flonicamid is an insecticide that acts rapidly and is considered as the only member of a new class of pesticides due to its special chemical structure. Therefore, a deep knowledge of its structural parameters as well as some related physicochemical aspects are mandatory. The potential reactivity of this compound has been revealed from the calculated structural properties, spectroscopic data, and reactivity results. The conformational search for flonicamid showed eight most stable conformers at M06-2X/6-311+G(d,p) level of theory, considering calculations with solvent (water) implemented by PCM. The molecular structure of flonicamid could exhibits conformational isomerism due to four dihedral angles. One of them is related with the rotation of groups around the C–CF_3 bond for which the (±*ac*) conformation was always observed in the as-obtained conformers. A second dihedral angle is associated with the conformation of the amide group, which is not completely rotational-free due to the double bond character of the C–N bond. Therefore,

the eight most stable conformers exhibited the *trans* stereochemistry around this bond. The other two dihedral angles are C10–C3–C8–O16 and H20–N15–C17–H21 for which a simultaneous scan leads to eight areas of minimum energy in the Potential Energy Surface of the molecule. On the other hand, these results perfectly agree with the fact that each of the eight molecular geometries found in the conformational search belongs to one of these zones of minimum energy, validating the implemented methodology.

Vibrational modes were assigned to the 60 calculated vibration frequencies and the calculated IR frequencies at B3LYP/6-311+G(d,p) and M06-2X/6-311+G(d,p) agrees well with the experimental spectrum reported previously.

The electronic absorption properties of flonicamid indicated that this molecule is active in the UV region, showing two predominant signals in the respective spectrum. The less energetic electronic transition (4.41 eV) can be attributed to a n→π* transition composed by two electronic excitations from HOMO to LUMO and from HOMO-1 to LUMO.

On the other hand, the Molecular Electronic Potential, the $f^{-}(\boldsymbol{r})$ and $\Delta f(\boldsymbol{r})$, altogether predicted the electrophilic attack predominantly around the N5 and O16 region, and secondarily in N15, N19 and the pyridine ring (at positions C2 and C4). Any other way, $f^{+}(\boldsymbol{r})$ and $\Delta f(\boldsymbol{r})$ predicted a nucleophilic attack along the aromatic ring, in respective sites for a nucleophilic aromatic substitution, according to the classical behavior of pyridine and other deactivated rings (deactivated for the electrophilic aromatic substitution). These results are also sustained by the corresponding condensed Fukui functions and condensed dual descriptors.

Finally, the docking results suggested strong DNA bindings for flonicamid and TFNA to the DNA, through hydrogen bonding and hydrophobic interactions. This suggests that there is a need to experimentally evaluate this pesticide and its main metabolites as possible carcinogens compounds. The DNA intercalant compounds generate DNA direct mutations. This work also shows that the affinity energy of flonicamid to DNA is like the one for ethidium bromide, which represents a danger for human health, Due to this and considering that flonicamid is usually spread outdoors in crops, the monitoring and promotion of its safety use among workers exposed to flonicamid herbicide, should be considered as a prudential practice, particularly for farmers and professional sprayers. Therefore, it is also mandatory and necessary to carried out studies on the risks of developing cancer from exposure to this pesticide and its metabolites.

SUPPLEMENTARY MATERIAL

Supplementary material related to this article can be found in the online version.

CRediT author statement

P. Corregidor: Conceptualization, Methodology, Investigation, Validation, Formal analysis, Writing-Original draft preparation & Editing, Visualization, Funding acquisition, Project administration, Supervision. **M. A. Zígolo**: Investigation, Docking methodology, Formal analysis, Docking essay, Writing-Original draft preparation & Editing, Visualization. **E. E. Ottavianelli**: Conceptualization, Formal analysis, Review & Editing, Supervision.

Declaration of interests

☒ The authors declare that they have no known competing financial interests or personal relationships that could have appeared to influence the work reported in this paper.

☐The authors declare the following financial interests/personal relationships which may be considered as potential competing interests:

ACKNOWLEDGMENTS

We are grateful for the financial support received as a grant from the Consejo de Investigación de la Universidad Nacional de Salta (Project N° 2546/0). SEAGrid platform (http:\www.seagrid.org) [42-44] is acknowledged for computational resources and services for the selected results used in this publication.

REFERENCES

[1] M. Morita, T. Ueda, T. Yoneda, T. Koyanagi, T. Haga, Flonicamid, a novel insecticide with a rapid inhibitory effect on aphid feeding, Pest Management Science, 63 (2007) 969-973.

[2] M. Morita, T. Yoneda, N. Akiyoshi, Research and development of a novel insecticide, flonicamid, Journal of Pesticide Science, 39 (2014) 179-180.

[3] J. Taylor-Wells, A.D. Gross, S. Jiang, F. Demares, J.S. Clements, P.R. Carlier, J.R. Bloomquist, Toxicity, mode of action, and synergist potential of flonicamid against mosquitoes, Pesticide Biochemistry and Physiology, (2018).

[4] S.J. Yu, The Classification of Insecticides, The Toxicology and Biochemistry of Insecticides
CRC Press, USA, 2011, pp. 25-86.

[5] M. Kumar, S. Jaiswal, R. Singh, G. Srivastav, P. Singh, T.N. Yadav, R.A. Yadav, Ab initio studies of molecular structures, conformers and vibrational spectra of heterocyclic organics: I. Nicotinamide and its N-oxide, Spectrochimica Acta Part A: Molecular and Biomolecular Spectroscopy, 75 (2010) 281-292.

[6] S. Ramalingam, S. Periandy, M. Govindarajan, S. Mohan, FT-IR and FT-Raman vibrational spectra and molecular structure investigation of nicotinamide: A combined experimental and theoretical study, Spectrochimica Acta Part A: Molecular and Biomolecular Spectroscopy, 75 (2010) 1552-1558.

[7] S.M. Soliman, R.A. Massoud, Theoretical studies of molecular structure and vibrational spectra of free, H-bonded and coordinated nicotinamide, Computational and Theoretical Chemistry, 988 (2012) 27-33.

[8] E.A. Velcheva, L.I. Daskalova, The experimental and computational study on the IR spectra and structure of pyridine-3-carboxamide (nicotinamide)-d0 and -d2, Journal of Molecular Structure, 741 (2005) 85-92.

[9] T. Takeshima, H. Takeuchi, T. Egawa, S. Konaka, Gas-phase molecular structure of nicotinamide studied by electron diffraction combined with MP2 calculations, Journal of Molecular Structure, 644 (2003) 197-205.

[10] G. Theodoridis, Chapter 4 Fluorine-Containing Agrochemicals: An Overview of Recent Developments, in: A. Tressaud (Ed.) Advances in Fluorine Science, Elsevier2006, pp. 121-175.

[11] N. Sakamoto, S. Saito, T. Hirose, M. Suzuki, S. Matsuo, K. Izumi, T. Nagatomi, H. Ikegami, K. Umeda, K. Tsushima, N. Matsuo, The discovery of pyridalyl: a novel insecticidal agent for controlling lepidopterous pests, Pest Management Science, 60 (2004) 25-34.

[12] M. Tsikolia, U.R. Bernier, M.R. Coy, K.C. Chalaire, J.J. Becnel, N.M. Agramonte, N. Tabanca, D.E. Wedge, G.G. Clark, K.J. Linthicum, D.R. Swale, J.R. Bloomquist, Insecticidal, repellent and fungicidal properties of novel trifluoromethylphenyl amides, Pesticide Biochemistry and Physiology, 107 (2013) 138-147.

[13] M. Gupta, A. Shanker, Fate of imidacloprid and acetamiprid residues during black tea manufacture and transfer into tea infusion, Food Additives & Contaminants: Part A, 26 (2009) 157-163.

[14] D.K. Sahu, J. Rai, M.K. Rai, M.K. Banjare, M. Nirmal, K. Wani, R. Sahu, S.G. Pandey, P. Mundeja, Detection of flonicamid insecticide in vegetable samples by UV–Visible spectrophotometer and FTIR, Results in Chemistry, 2 (2020) 100059.

[15] E.F.S. Authority, Conclusion on the peer review of the pesticide risk assessment of the active substance flonicamid, EFSA Journal, 8 (2010) 1445.

[16] H. Li, Q. Zhong, X. Wang, F. Luo, L. Zhou, H. Sun, M. Yang, Z. Lou, Z. Chen, X. Zhang, The degradation and metabolism of chlorfluazuron and flonicamid in tea: A risk assessment from tea garden to cup, Sci Total Environ, 754 (2021) 142070.

[17] I. Colomer, P. Aguado, P. Medina, R.M. Heredia, A. Fereres, J.E. Belda, E. Viñuela, Field trial measuring the compatibility of methoxyfenozide and flonicamid with Orius laevigatus Fieber (Hemiptera: Anthocoridae) and Amblyseius swirskii (Athias-Henriot) (Acari: Phytoseiidae) in a commercial pepper greenhouse, Pest Manag Sci, 67 (2011) 1237-1244.

[18] S.W. Lee, J.-H. Choi, S.-K. Cho, H.-A. Yu, A.M. Abd El-Aty, J.-H. Shim, Development of a new QuEChERS method based on dry ice for the determination of 168

pesticides in paprika using tandem mass spectrometry, Journal of Chromatography A, 1218 (2011) 4366-4377.

[19] S. Wang, F. Jin, X. Cao, Y. Shao, J. Wang, Y. She, Y. Qi, C. Zhang, H. Li, M. Jin, J. Wang, H. Shao, L. Zheng, Residue behaviors and risk assessment of flonicamid and its metabolites in the cabbage field ecosystem, Ecotoxicology and Environmental Safety, 161 (2018) 420-429.

[20] I. Hypercube, HyperChem Release 5.0 for Windows: Reference Manual, Hypercube, Incorporated 1996.

[21] A.R. Katritzky, M. Szafran, E. Anders, N. Malhotra, S.U. Chaudry, Aromaticity as a quantitative concept part V: A comparison of semi-empirical methods for the calculation of molecular geometries of heteroaromatic compounds and application of the AM1 and MNDO methods to the calculation of Bird's aromaticity indices, Tetrahedron Computer Methodology, 3 (1990) 247-269.

[22] R.O. Jones, O. Gunnarsson, The density functional formalism, its applications and prospects, Reviews of Modern Physics, 61 (1989) 689-746.

[23] S.H. Vosko, L. Wilk, M. Nusair, Accurate spin-dependent electron liquid correlation energies for local spin density calculations: a critical analysis, Canadian Journal of Physics, 58 (1980) 1200-1211.

[24] D.M. Ceperley, B.J. Alder, Ground State of the Electron Gas by a Stochastic Method, Physical Review Letters, 45 (1980) 566-569.

[25] C. Lee, W. Yang, R.G. Parr, Development of the Colle-Salvetti correlation-energy formula into a functional of the electron density, Physical Review B, 37 (1988) 785-789.

[26] A.D. Becke, Density- functional thermochemistry. III. The role of exact exchange, The Journal of Chemical Physics, 98 (1993) 5648-5652.

[27] Y. Zhao, D.G. Truhlar, The M06 suite of density functionals for main group thermochemistry, thermochemical kinetics, noncovalent interactions, excited states, and

transition elements: two new functionals and systematic testing of four M06-class functionals and 12 other functionals, Theoretical Chemistry Accounts, 120 (2008) 215-241.

[28] B.P. Pritchard, D. Altarawy, B. Didier, T.D. Gibson, T.L. Windus, New Basis Set Exchange: An Open, Up-to-Date Resource for the Molecular Sciences Community, Journal of Chemical Information and Modeling, 59 (2019) 4814-4820.

[29] K.L. Schuchardt, B.T. Didier, T. Elsethagen, L. Sun, V. Gurumoorthi, J. Chase, J. Li, T.L. Windus, Basis Set Exchange: A Community Database for Computational Sciences, Journal of Chemical Information and Modeling, 47 (2007) 1045-1052.

[30] M.D. Hanwell, D.E. Curtis, D.C. Lonie, T. Vandermeersch, E. Zurek, G.R. Hutchison, Avogadro: an advanced semantic chemical editor, visualization, and analysis platform, Journal of Cheminformatics, 4 (2012) 17.

[31] M.P. Andersson, P. Uvdal, New Scale Factors for Harmonic Vibrational Frequencies Using the B3LYP Density Functional Method with the Triple-ζ Basis Set 6-311+G(d,p), The Journal of Physical Chemistry A, 109 (2005) 2937-2941.

[32] J. Zheng, D.G. Truhlar, 2014.

[33] M.H. Jamróz, Vibrational Energy Distribution Analysis VEDA 4, Warsaw, (2004-2010).

[34] M.H. Jamróz, Vibrational Energy Distribution Analysis (VEDA): Scopes and limitations, Spectrochimica Acta Part A: Molecular and Biomolecular Spectroscopy, 114 (2013) 220-230.

[35] S. Das, A. Chakraborty, Conformer selective monohydrated clusters of 1,2,3,4 – tetrahydroisoquinoline in S0: I-Potential energy surface studies, vibrational signatures and NBO analysis, Journal of Molecular Structure, 1225 (2021) 129177.

[36] I. Sayer, N. Dege, H. Ghalla, A. Moliterni, H. Naïli, Crystal structure, DFT studies and thermal characterization of new luminescent stannate (IV) based inorganic-organic hybrid compound, Journal of Molecular Structure, 1224 (2021) 129266.

[37] C. Sivakumar, V. Balachandran, B. Narayana, V.V. Salian, B. Revathi, N. Shanmugapriya, K. Vanasundari, Molecular spectroscopic investigation, quantum chemical, molecular docking and biological evaluation of 2-(4-Chlorophenyl)-1-[3-(4-chlorophenyl)-5-[4-(propan-2-yl) phenyl-3, 5-dihydro-1H-pyrazole-yl] ethanone, Journal of Molecular Structure, 1224 (2021) 129010.

[38] Y. Sert, L.M. Singer, M. Findlater, H. Doğan, Ç. Çırak, Vibrational frequency analysis, FT-IR, DFT and M06-2X studies on tert-Butyl N-(thiophen-2yl)carbamate, Spectrochimica Acta Part A: Molecular and Biomolecular Spectroscopy, 128 (2014) 46-53.

[39] T. Lu, F. Chen, Multiwfn: A multifunctional wavefunction analyzer, Journal of Computational Chemistry, 33 (2012) 580-592.

[40] B. Wang, C. Rong, P.K. Chattaraj, S. Liu, A comparative study to predict regioselectivity, electrophilicity and nucleophilicity with Fukui function and Hirshfeld charge, Theoretical Chemistry Accounts, 138 (2019) 124.

[41] M.J. Frisch, G.W. Trucks, H.B. Schlegel, G.E. Scuseria, M.A. Robb, J.R. Cheeseman, G. Scalmani, V. Barone, G.A. Petersson, H. Nakatsuji, X. Li, M. Caricato, A.V. Marenich, J. Bloino, B.G. Janesko, R. Gomperts, B. Mennucci, H.P. Hratchian, J.V. Ortiz, A.F. Izmaylov, J.L. Sonnenberg, Williams, F. Ding, F. Lipparini, F. Egidi, J. Goings, B. Peng, A. Petrone, T. Henderson, D. Ranasinghe, V.G. Zakrzewski, J. Gao, N. Rega, G. Zheng, W. Liang, M. Hada, M. Ehara, K. Toyota, R. Fukuda, J. Hasegawa, M. Ishida, T. Nakajima, Y. Honda, O. Kitao, H. Nakai, T. Vreven, K. Throssell, J.A. Montgomery Jr., J.E. Peralta, F. Ogliaro, M.J. Bearpark, J.J. Heyd, E.N. Brothers, K.N. Kudin, V.N. Staroverov, T.A. Keith, R. Kobayashi, J. Normand, K. Raghavachari, A.P. Rendell, J.C. Burant, S.S. Iyengar, J. Tomasi, M. Cossi, J.M. Millam, M. Klene, C. Adamo, R. Cammi, J.W. Ochterski, R.L. Martin, K. Morokuma, O. Farkas, J.B. Foresman, D.J. Fox, Gaussian 16 Rev. C.01, Wallingford, CT, 2016.

[42] R. Dooley, K. Milfeld, C. Guiang, S. Pamidighantam, G. Allen, From Proposal to Production: Lessons Learned Developing the Computational Chemistry Grid Cyberinfrastructure, J. Grid. Comput., 4 (2006) 195.

[43] S. Pamidighantam, S. Nakandala, E. Abeysinghe, C. Wimalasena, S.R. Yodage, S. Marru, M. Pierce, Community Science Exemplars in Seagrid Science Gateway: Apache Airavata Based Implementation of Advanced Infrastructure, Procedia Comput. Sci., 80 (2016) 1927.

[44] N. Shen, Y. Fan, S. Pamidighantam, E-Science Infrastructures for Molecular Modeling and Parametrization, J. Comput. Sci., 5 (2014) 576.

[45] H.R. Drew, R.M. Wing, T. Takano, C. Broka, S. Tanaka, K. Itakura, R.E. Dickerson, Structure of a B-DNA dodecamer: conformation and dynamics, Proceedings of the National Academy of Sciences, 78 (1981) 2179-2183.

[46] G.M. Morris, D.S. Goodsell, R.S. Halliday, R. Huey, W.E. Hart, R.K. Belew, A.J. Olson, Automated docking using a Lamarckian genetic algorithm and an empirical binding free energy function, Journal of Computational Chemistry, 19 (1998) 1639-1662.

[47] W.J. Hehre, L. Radom, J.A. Pople, Molecular orbital theory of the electronic structure of organic compounds. XII. Conformations, stabilities, and charge distributions in monosubstituted benzenes, Journal of the American Chemical Society, 94 (1972) 1496-1504.

[48] N. Choudhary, P. Agarwal, A. Gupta, P. Tandon, Quantum chemical calculations of conformation, vibrational spectroscopic, electronic, NBO and thermodynamic properties of 2,2-dichloro-N-(2,3-dichlorophenyl) acetamide and 2,2-dichloro-N-(2,3-dichlorophenyl) acetamide, Computational and Theoretical Chemistry, 1032 (2014) 27-41.

[49] B. Karasulu, W. Thiel, Photoinduced Intramolecular Charge Transfer in an Electronically Modified Flavin Derivative: Roseoflavin, The Journal of Physical Chemistry B, 119 (2015) 928-943.

[50] F. Parker, Amides and Amines, Applications of Infrared Spectroscopy in Biochemistry, Biology, and Medicine
Springer US, New York, 2012, pp. 165-172.

[51] S.-i. Mizushima, T. Simanouti, S. Nagakura, K. Kuratani, M. Tsuboi, H. Baba, O. Fujioka, The Molecular Structure of N-Methylacetamide, Journal of the American Chemical Society, 72 (1950) 3490-3494.

[52] R. Jones, R. Rao, Infrared absorption of some 3,4-disubstituted pyridines and pyridine 1-oxides, Australian Journal of Chemistry, 18 (1965) 583-587.

[53] E.B. Wilson, The Normal Modes and Frequencies of Vibration of the Regular Plane Hexagon Model of the Benzene Molecule, Physical Review, 45 (1934) 706-714.

[54] J. Laxman Naik, B. Venkatram Reddy, N. Prabavathi, Experimental (FTIR and FT-Raman) and theoretical investigation of some pyridine-dicarboxylic acids, Journal of Molecular Structure, 1100 (2015) 43-58.

[55] R.A. Yadav, S. Singh, Vibrational spectra and normal coordinate analysis for substituted trifluoromethyl benzenes, Proceedings of the Indian Academy of Sciences (Chemical Sciences), 95 (1985) 471-487.

[56] T.K. Gounev, G.A. Guirgis, J.R. Durig, Vibrational spectra, conformational stability and ab initio calculations of trifluoromethylsulfonyl isocyanate, Journal of Molecular Structure, 436-437 (1997) 613-625.

[57] J.E. Galván, E. Contreras Aguilar, M.E. Defonsi Lestard, M.E. Tuttolomondo, S.E. Ulic, A. Ben Altabef, Theoretical and experimental study of a new thiosulfonate derivative: Methyl trifluoromethanethiosulfonate, CF3SO2SCH3. Conformational transferability in CX3SO2S-R compounds, Inorganica Chimica Acta, 455 (2017) 254-261.

[58] S.S. Stoyanov, Scaling of Computed Cyano-Stretching Frequencies and IR Intensities of Nitriles, Their Anions, and Radicals, The Journal of Physical Chemistry A, 114 (2010) 5149-5161.

[59] P. Hohenberg, W. Kohn, Inhomogeneous Electron Gas, Physical Review, 136 (1964) B864-B871.

[60] J.-i. Aihara, Weighted HOMO-LUMO energy separation as an index of kinetic stability for fullerenes, Theoretical Chemistry Accounts, 102 (1999) 134-138.

[61] K.H. Kim, Y.-K. Han, J. Jung, Basis set effects on relative energies and HOMO–LUMO energy gaps of fullerene C36, Theoretical Chemistry Accounts, 113 (2005) 233-237.

[62] E. Scrocco, J. Tomasi, Electronic Molecular Structure, Reactivity and Intermolecular Forces: An Euristic Interpretation by Means of Electrostatic Molecular Potentials, in: P.-O. Löwdin (Ed.) Advances in Quantum Chemistry, Academic Press1978, pp. 115-193.

[63] S.J. Grabowski, J. Leszczynski, Unrevealing the Nature of Hydrogen Bonds: π-Electron Delocalization Shapes H-Bond Features. Intramolecular and Intermolecular Resonance-Assisted Hydrogen Bonds, in: S.J. Grabowski (Ed.) Hydrogen Bonding—New Insights, Springer Netherlands, Dordrecht, 2006, pp. 487-512.

[64] E. Scrocco, J. Tomasi, The electrostatic molecular potential as a tool for the interpretation of molecular properties, Springer Berlin Heidelberg, Berlin, Heidelberg, 1973, pp. 95-170.

[65] K. Fukui, Role of Frontier Orbitals in Chemical Reactions, Science, 218 (1982) 747-754.

[66] G. Bottegoni, W. Rocchia, M. Recanatini, A. Cavalli, AClAP, Autonomous hierarchical agglomerative Cluster Analysis based protocol to partition conformational datasets, Bioinformatics, 22 (2006) e58–e65.

[67] R. Huey, G.M. Morris, A.J. Olson, D.S. Goodsell, A semiempirical free energy force field with charge-based desolvation, Journal of Computational Chemistry, 28 (2007) 1145-1152.

[68] G.M. Morris, R. Huey, W. Lindstrom, M.F. Sanner, R.K. Belew, D.S. Goodsell, A.J. Olson, AutoDock4 and AutoDockTools4: Automated docking with selective receptor flexibility, Journal of Computational Chemistry, 30 (2009) 2785-2791.

[69] C. Bolognesi, F.D. Merlo, Pesticides: Human Health Effects☆, in: J. Nriagu (Ed.) Encyclopedia of Environmental Health (Second Edition), Elsevier, Oxford, 2019, pp. 118-132.